



Article

Alkoxy-Functionalized Schiff-Base Ligation at Aluminum and Zinc: Synthesis, Structures and ROP Capability

Xin Zhang ¹, Kai Chen ², Melissa Chicoma ³, Kimberly Goins ³, Timothy J. Prior ¹ , Terence A. Nile ^{3,*} and Carl Redshaw ^{1,*} 

¹ Plastics Collaboratory, Department of Chemistry, University of Hull, Cottingham Road, Hull HU6 7RX, UK; x.zhang-2019@hull.ac.uk (X.Z.); t.prior@hull.ac.uk (T.J.P.)

² Collaborative Innovation Center of Atmospheric Environment and Equipment Technology, Jiangsu Key Laboratory of Atmospheric Environment Monitoring and Pollution Control, School of Environmental Science and Engineering, Nanjing University of Information Science & Technology, Nanjing 210044, China; kaichen85@nuist.edu.cn

³ Department of Chemistry, University of North Carolina Greensboro, Greensboro, NC 27402-6170, USA; m.chicoma33@gmail.com (M.C.); kngoins2@alumni.uncg.edu (K.G.)

* Correspondence: terry_nile@uncg.edu (T.A.N.); c.redshaw@hull.ac.uk (C.R.)

Abstract: The Schiff-base compounds 2,4-di-*tert*-butyl-6-(((3,4,5-trimethoxyphenyl)imino)methyl)phenol (L¹H), 2,4-di-*tert*-butyl-6-(((2,4,6-trimethoxyphenyl)imino)methyl)phenol (L²H), 2,4-di-*tert*-butyl-6-(((2,4-trimethoxyphenyl)imino)methyl)phenol (L³H) derived from anilines bearing methoxy substituents have been employed in the preparation of alkylaluminum and zinc complexes. Molecular structure determinations reveal mono-chelate aluminum complexes of the type [Al(Lⁿ)(Me)₂] (L¹, **1**; L², **2**; L³, **3**), and bis(chelate) complexes for zinc, namely [Zn(Lⁿ)₂] (L¹, **5**; L², **6**; L³, **7**). All complexes have significant activity at 50 °C and higher activity at 100 °C for the ring-opening polymerization (ROP) of ϵ -caprolactone (ϵ -CL) with good control over the molar mass distribution ($M_w/M_n < 2$) and molecular weight. Complex **1** was found to be the most active catalyst, achieving 99% conversion within 18 h at 50 °C and giving polycaprolactone with high molecular weight; results are compared against aniline-derived (i.e., non-methoxy containing) complexes (**4** and **8**). Aluminum or zinc complexes derived from L¹ exhibit higher activity as compared with complexes derived from L² and L³. Complex **1** was also tested as an initiator for the copolymerization of ϵ -CL and glycolide (GL). The CL-GL copolymers have various microstructures depending on the feed ratio. The crosslinker 4,4'-bioxepane-7,7'-dione was used in the polymerization with ϵ -CL using **1**, and well-defined cross-linked PCL was afforded of high molecular weight.

Keywords: Schiff base; organoaluminum; zinc; catalyst; polycaprolactone; copolymer; ring-opening polymerization; molecular structures



Citation: Zhang, X.; Chen, K.; Chicoma, M.; Goins, K.; Prior, T.J.; Nile, T.A.; Redshaw, C. Alkoxy-Functionalized Schiff-Base Ligation at Aluminum and Zinc: Synthesis, Structures and ROP Capability. *Catalysts* **2021**, *11*, 1090. <https://doi.org/10.3390/catal11091090>

Academic Editor: Samuel Dagorne

Received: 14 August 2021

Accepted: 3 September 2021

Published: 9 September 2021

Publisher's Note: MDPI stays neutral with regard to jurisdictional claims in published maps and institutional affiliations.



Copyright: © 2021 by the authors. Licensee MDPI, Basel, Switzerland. This article is an open access article distributed under the terms and conditions of the Creative Commons Attribution (CC BY) license (<https://creativecommons.org/licenses/by/4.0/>).

1. Introduction

The use of Schiff-base, or as it is sometimes called phenoxyimine (FI) ligation in metal-based catalysis, has seen some notable successes in recent years. For example, in α -olefin polymerization, researchers at the Mitsui Chemical Corp. achieved both increased thermal stability and very high activity for vanadium-based systems of the type [VO(FI)₂] [1]. The use of pendant functionality has also proved to be an area of promise [2]. As catalysis researchers have turned their attention to more potentially environmentally-benign polymers, the use of Schiff-base ligation has remained a central theme. In particular, their use in the ring opening polymerization (ROP) of cyclic esters has led to catalysts employing the metals aluminum and zinc [3–7]. Given that the sterics and electronics associated with the coordination geometry at the metal allows for the manipulation of the ROP process, numerous combinations of different Schiff-base ligands have been studied. However, the use of Schiff-base ligands bearing multiple alkoxy substituents is limited, despite the ready

availability of suitable precursors. In related chemistry, Guo [8] previously reported iron(II) 2,6-bis(imino)pyridyl complexes bearing bulky *para* substituents ($R = \text{CH}_3, \text{OCH}_3$) at the aniline and their catalytic properties in ethylene polymerization. It was found that the electron-donating methoxy substituent resulted in a slight decrease of catalytic activity, but a significant increase of molecular weight compared with the methyl analogue. Ghaffari [9] has also investigated the position effects (*ortho*, *meta*, *para*) of methoxy substituents for nickel(II) complexes and utilized such complexes for the epoxidation of cyclooctene. We note that in salen-based nickel chemistry, the presence of the methoxy substituents has led to enhanced activity and increased selectivity for epoxidations. Thus, herein we have initiated a program to screen Schiff-base ligands derived from anilines bearing alkoxy substituents. The effect on the catalytic activity of the ROP of cyclic esters of different substitution patterns for the electron-donating methoxy substituent groups at the aniline derived moiety of bidentate *N,O*-Schiff base is investigated. It is desirable that the catalyst is cheap and readily accessible and so we have focused our studies on the earth abundant metals aluminum and zinc. The use of main-group metal ROP catalysts has been reviewed [3,5], and other reviews have focused on the use of aluminum [4,6] and more recently Schiff-base ligation [7].

2. Results and Discussion

2.1. Synthesis and Characterization of Schiff-Base Aluminum Complexes

The organoaluminum complexes **1**, **2** and **3**, bearing the phenoxy-imines L^1 , L^2 and L^3 respectively, were prepared by reaction of AlMe_3 with one equivalent of the parent phenoxyimine ($L^1\text{H} = 2,4\text{-di-}t\text{-butyl-6-}(((3,4,5\text{-trimethoxyphenyl})\text{imino})\text{methyl})\text{phenol}$, $L^2\text{H} = 2,4\text{-di-}t\text{-butyl-6-}(((2,4,6\text{-trimethoxyphenyl})\text{imino})\text{methyl})\text{phenol}$ and $L^3\text{H} = 2,4\text{-di-}t\text{-butyl-6-}(((2,4\text{-trimethoxyphenyl})\text{imino})\text{methyl})\text{phenol}$) in toluene. These reactions took place along with the evolution of methane [10], and following work-up, analytically pure yellow needle-shaped crystals were collected from the saturated solution of acetonitrile at 5°C in 52% (**1**), 34% (**2**), 64% (**3**) yields, respectively. In the ^1H NMR spectra of **1-3**, a sharp single resonance is ascribed to the Al-Me_2 protons at -0.79 , -1.00 , -0.93 ppm, respectively, and a resonance ascribed to the CH=N proton at 8.82 ppm for **1**, 8.58 ppm for **2**, or 8.58 ppm for **3** observed, see Figure S1.

The molecular structures of **1**, **2** and **3** were further verified by X-ray diffraction studies (Figure 1 and Table 1). The Al centers in **1**, **2** and **3** are four-coordinate with a bidentate *N,O*-chelate and two methyl ligands. **1** crystallizes in space group $P4_2/n$ with coordination geometry around the metal center described as distorted tetrahedral; angles range from $94.59(10)$ to $119.12(16)^\circ$. The most “acute” angle is associated with the bite angle of the chelate ligand [$94.59(10)^\circ$], which is close to those previously reported for $[\text{L}^{\text{ClBu}}\text{-AlMe}_2(5)]$ [$93.32(6)^\circ$] [11] ($\text{L}^{\text{ClBu}} = 4\text{-ClC}_6\text{H}_4\text{CH=NN=CHC}_6\text{H}_2\text{-2-(O)-3,5-}t\text{Bu}$) and $\text{Me}_2\text{Al}[\text{O-2-Me-6-(R}_2\text{N=CH)C}_6\text{H}_3]$ [$\text{R}_2=2,6\text{-}i\text{Pr}_2\text{C}_6\text{H}_3$] [$93.68(7)^\circ$] [12], $[\text{Me}_2\text{AlL}^{\text{hyd}}]$ ($\text{L}^{\text{hyd}}\text{H} = 2,4\text{-di-}t\text{-butyl-6-(2,6-dibenzylhydridyl-4-isopropylphenylimino)methylphenol}$) [$94.14(8)^\circ$] [13]. The Al–C bond distances in **1** [Al(1)–C(22) $1.955(4)$ Å, Al(1)–C(23) $1.961(3)$ Å] are typical, while the Al(1)–O(1) bond length is [$1.765(2)$ Å], indicative of a σ -bond [13]. The Al(1)–N(1) bond distance in **1** [$1.980(3)$ Å] is longer than those in $[\text{Me}_2\text{NC}(\text{NiPr})_2\text{AlCl}_2]$ [$1.872(3)$ Å] [14], consistent with dative type bonding.

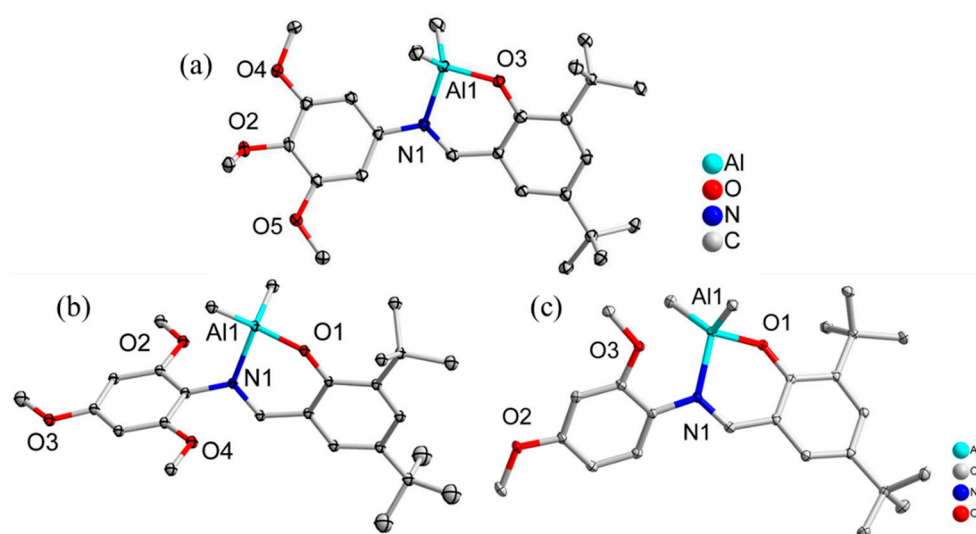


Figure 1. ORTEP drawing (20% probability) of complexes (a) $[\text{Al}(\text{L}^1)(\text{Me})_2]$ (**1**); (b) $[\text{Al}(\text{L}^2)(\text{Me})_2]$ (**2**); (c) $[\text{Al}(\text{L}^3)(\text{Me})_2]$ (**3**). Hydrogen atoms are omitted for clarity.

Table 1. Selected bond lengths (Å) and angles (°) for the complexes **1–3**, **5–7**.

-	1	2	3	-	5	6	7
<i>Bond length (Å)</i>	-	-	-	-	-	-	-
Al(1)–O(1)	1.7650(2)	1.7895(11)	1.8038(8)	Zn(1)–O(1)	1.9077(15)	1.9335(19)	1.9583(17)
Al(1)–C(22)	1.9550(4)	1.9592(17)	1.9626(12)	Zn(1)–O(2)	1.9088(15)	1.9338(18)	1.9573(18)
Al(1)–C(23)	1.9610(3)	1.9614(17)	1.9652(12)	Zn(1)–N(1)	1.9998(18)	2.026(2)	2.027(3)
Al(1)–N(1)	1.9800(3)	1.9570(14)	1.9923(10)	Zn(1)–N(2)	2.0089(18)	2.032(2)	2.026(2)
<i>Bond angles (°)</i>	-	-	-	-	-	-	-
O(1)–Al(1)–C(22)	109.08(14)	109.00(6)	107.68(5)	O(1)–Zn(1)–O(2)	122.14(7)	97.45(8)	117.54(8)
O(1)–Al(1)–C(23)	113.48(13)	112.77(6)	105.41(4)	O(1)–Zn(1)–N(1)	96.84(7)	93.54(9)	101.30(8)
C(22)–Al(1)–C(23)	119.12(16)	121.35(7)	123.31(5)	O(2)–Zn(1)–N(1)	111.25(7)	146.25(9)	91.96(9)
O(1)–Al(1)–N(1)	94.59(10)	93.74(5)	91.19(4)	O(1)–Zn(1)–N(2)	111.20(7)	138.49(8)	92.29(8)
C(22)–Al(1)–N(1)	108.91(13)	110.62(7)	111.29(5)	O(2)–Zn(1)–N(2)	95.76(7)	92.70(8)	105.58(9)
C(23)–Al(1)–N(1)	108.81(13)	105.78(7)	112.63(5)	N(1)–Zn(1)–N(2)	121.63(7)	99.93(8)	149.77(9)

The structure of **2** is similar to **1**, with a distorted four-coordinate metal center in the triclinic space group $P\bar{1}$. The O(4)–Al(1)–C(25) [109.00(6)°], O(4)–Al(1)–C(26) [112.77(6)°] and O(4)–Al(1)–N(1) [93.74(5)°] bond angles are smaller than those in **1** [109.08(14)°, 113.34(13)°, 94.59(10)°, respectively], whereas the angles C(25)–Al(1)–C(26) [121.35(7)°] and N(1)–Al(1)–C(25) [110.62(7)°] are larger than those in **1** [119.12(16)° and 108.91(13)°, respectively]. The Al–O distance in **2** [1.7895(11) Å] is longer than in **1** [1.765(2) Å] and the Al–N distance [1.9570(14) Å] is shorter than in **1** [1.980(3) Å]. The observed differences can be ascribed to the differing positions, and hence steric influence, of the substituents on the aniline derived moiety. The geometry in **3** resembles that in **2**. All pertinent bond distances around the Al center are close to those in **2**, except the distance of Al(1)–N(1) [1.9923(10) Å] in **3** is longer than **2** [1.9570(14) Å]. The bond angles around the Al atom range from 91.19(4)° to 123.31(5)°.

The IR spectrum of **1** contains an absorption band at 1613 cm^{-1} assigned to $\nu(\text{C}=\text{N})$. The $\nu(\text{C}=\text{N})$ band of the parent L^1H is found at 1614 cm^{-1} , which is consistent with the observation of Sarma and Bailar [15] who reported no shift in $\nu(\text{C}=\text{N})$ bond frequency even after complexation. The coordination of the azomethine nitrogen is further supported by the appearance of new band at 587 cm^{-1} due to $\nu(\text{Al}-\text{N})$. The stretching vibration observed at 1249 cm^{-1} is attributed to the phenolic C–O vibration of L^1 [16]. For **1**, the shift of this band to lower frequency at 1237 cm^{-1} indicates the bonding of the ligand to the metal atom through oxygen. The formation of the Al–O bond was supported by the

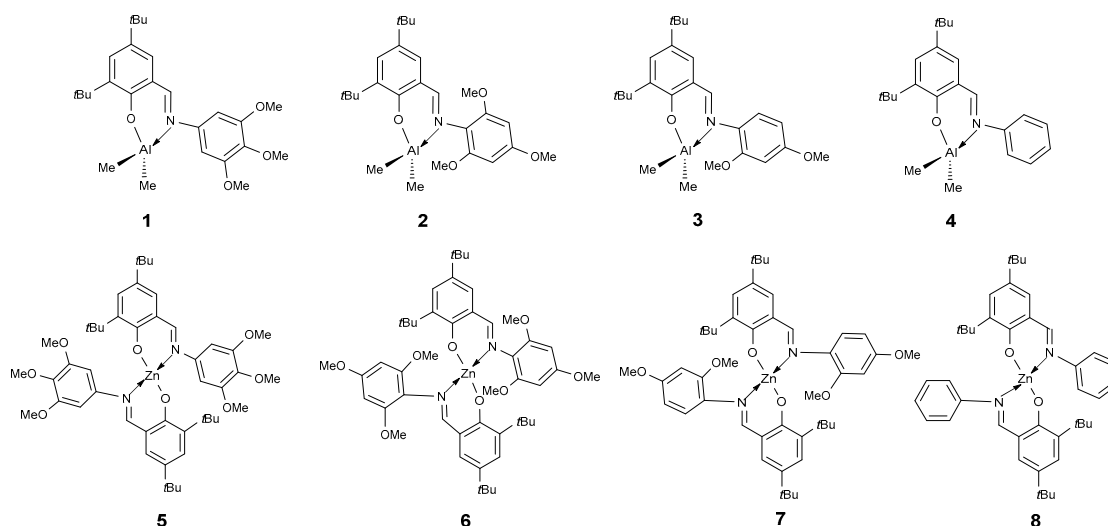
appearance of medium bands in the region of 708 cm^{-1} . The absorption at 609 cm^{-1} is assigned to $\nu(\text{Al-C})$ [17]. The IR spectra for **2** and **3** are similar to **1**. The strong absorption at 1614 cm^{-1} was assigned to $\nu(\text{C=N})$ stretching. Compared to the free ligand (1619 cm^{-1}), the $\nu(\text{C=N})$ stretching of **2** is slightly shifted to lower frequency. The important IR bands are summarized in Table 2. The solid-state structures of the aluminum complexes **1–3** are consistent with their ^1H NMR spectra, elemental analysis and mass spectrometry data.

Table 2. Some relevant IR spectral data of complexes **1–3**, **5–7** and L^{1-3}H (cm^{-1}).

-	$\nu(\text{C=N})$	$\nu(\text{C-O})$	$\nu(\text{M-O})$	$\nu(\text{M-N})$	$\nu(\text{Al-C})$
1	1613	1237	708	587	609
2	1614	1230	705	575	604
3	1615	1240	755	579	676
5	1612	1237	661	598	-
6	1614	1227	687	571	-
7	1616	1258	-	-	-
L^1H	1614	1249	-	-	-
L^2H	1619	1230	-	-	-
L^3H	1616	1250	-	-	-

2.2. Synthesis and Characterization of Schiff-Base Zinc Complexes

The reaction of L^1H , L^2H or L^3H with one equivalent of ZnEt_2 in refluxing toluene readily afforded the bis(chelate) complexes **5**, **6** and **7** (Scheme 1), respectively. Analytically pure yellow prisms were collected, following work-up, from a saturated solution of acetonitrile at 5°C in 48% (**5**), 40% (**6**) or 60% (**7**) yields, respectively. In the ^1H NMR spectra of **5**, **6** or **7**, a resonance is ascribed to the CH=N proton at 8.65 ppm for **5**, 8.36 ppm for **6**, or 8.50 ppm for **7** (see Figure S2).



Scheme 1. Structures of the aluminum and zinc complexes **1–8** prepared herein.

The molecular structures of **5**, **6** and **7** are presented in Figure 2. Selected bond lengths and angles are collated in Table 1; crystallographic data are collated in Appendix A. **5** crystallizes in the orthorhombic space group $Pbca$ and each Zn center in **5** is distorted tetrahedral with two N and two O atoms from two Schiff-base ligands L^1 , with angles ranging from $95.76(7)$ – $121.63(7)^\circ$, which are comparable with others reported for analogous square planar Zn(II) species [18,19]. The average bond distances for the Zn(1)-(O) and Zn(1)-(N) bonds are $[1.908\text{ \AA}]$ and $[2.004\text{ \AA}]$, respectively, which are comparable with previous reported values [20–23]. The metal ion in **6** (monoclinic space group $I2/a$), also adopts a distorted tetrahedral geometry for which the O(1)-Zn(1)-N(1) $[93.54(9)^\circ]$, O(2)-

Zn(1)–N(2) [92.70(8)] and O(2)–Zn(1)–O(1) [97.45(8)°], N(1)–Zn(1)–N(2) [99.93(8)°] bond angles are smaller than those in **5** [96.84(7)°, 95.76(7)°, 122.14(7)°, 121.63(7)°, respectively]. Moreover, the O(2)–Zn(1)–N(1) [146.25(9)°], O(1)–Zn(1)–N(2) [138.49(9)°] bond angles in **6** are larger than those in **5** [111.25(7)° and 111.20(7)° respectively], whilst the Zn–O [1.9338 Å] and Zn–N [2.026 Å] distances in **6** are longer than in **5** [1.9088 Å, 2.0089 Å]. The observed differences are attributed to the different positions of the methoxy substituents in the aniline derived group.

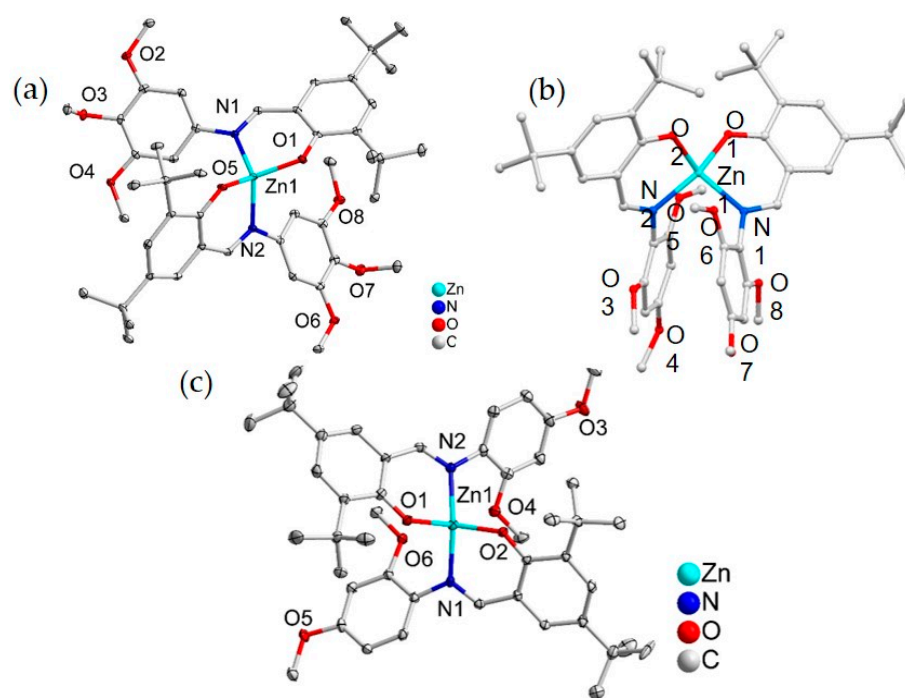


Figure 2. ORTEP drawing (20% probability) of complexes (a) [Zn(L¹)₂] (**5**); (b) [Zn(L²)₂] (**6**); (c) [Zn(L³)₂] (**7**). Hydrogen atoms are omitted for clarity.

Structure **7** also contains a Zn(II) center ligated by two L³ ligands similar to **5** and **6**. The two methoxy oxygens O(4) and O(6) are at a distance >2.5 Å from the zinc center and so are not considered as interacting. Given this, the zinc ion in **7** (monoclinic space group *P*2₁/*n*) also adopts a distorted tetrahedral geometry involving atoms O(1), O(2), N(1) and N(2). The bond lengths for Zn–O(1), Zn–O(2), Zn–N(1) are 1.9583(17), 1.9573(18), 2.027(3) Å, respectively, which are longer than observed in **5** and **6**; selected bond lengths and bond angles are collected in Table 1. The bond length for Zn(1)–N(2) [2.026(2) Å] in **7** is shorter than that in **6** [2.032(2) Å]. All of the O(1)–Zn(1)–O(2), N(1)–Zn(1)–N(2) angles are smaller than 180° causing the distorted tetrahedral geometry. In particular, the O(1)–Zn(1)–O(2) bond angle [117.54(8)°] in **7** is in the between of **5** [122.14(7)°] and **6** [97.45(8)°]. However, the N(1)–Zn(1)–N(2) bond angle [149.77(9)°] in **7** is much bigger than those in **5** [121.63(7)°] and **6** [99.93(8)°].

The infrared spectra of the complexes **5**, **6** and **7** are collected in Table 2 and are compared with that of free ligand to verify the bonding in the complexes. The band in the IR spectrum of L¹ at 1614 cm^{−1} (C=N) is shifted to slightly lower frequencies at 1612 cm^{−1} in **5**, indicating donation of the lone pair of electrons at the azomethine nitrogen to the zinc center [24]. Moreover, the coordination of the azomethine nitrogen is further supported by the appearance of new band at 598 cm^{−1} assigned to ν (Zn–N). The stretching vibration observed at 1249 cm^{−1} is attributed to the phenolic C–O vibration of L¹ [16]. In the complex **5**, the shift to lower frequency at 1237 cm^{−1} indicates the bonding of the ligand to the metal via oxygen. A new band for **5** at 661 cm^{−1} is assigned to ν (Zn–O); the IR spectrum for **6** and **7** is similar to **5**. Selected IR bands are summarized in the Table 2. The structures of the

zinc complexes **5–7** were consistent with their ^1H NMR spectra, elemental analysis and mass spectrometry data.

3. Ring Opening Polymerization (ROP)

3.1. Ring Opening Polymerization of ϵ -Caprolactone (ϵ -CL)

Complexes **1–8** have been screened for their ability to act as catalysts, in the presence of benzyl alcohol (BnOH), for the ROP of ϵ -caprolactone and the results are presented in Table 3. Results for **1–3** and **5–7** are compared against the related non-methoxy containing complexes **4** [25] and **8**, respectively. The polymerization reactions were carried out at 100 °C, using a [CL]:[catalyst]:[BnOH] ratio of 250:1:1. All complexes were found to be active under these polymerization conditions with similar monomer conversions (>95%) over different times. The aluminum complex **1** was capable of achieving 99% conversion in 40 min., whereas 120, 100 and 120 min. were required for **2**, **3** and **4**, respectively (Table 3, entries 1–4). In addition, **1** afforded a larger molecular weight ($M_n = 17,000$) compared with **2** ($M_n = 16,000$), **3** ($M_n = 16,000$) and **4** ($M_n = 12,000$), and narrow polydispersity indexes (**1**: PDI = 1.74) vs. **2** (PDI = 1.87), **3** (PDI = 1.90) and **4** (PDI = 2.41). The results herein indicated that ligands derived from anilines bearing 3,4,5-methoxy substituents favored the ROP process in terms of rate, molecular weight and control. Looking at the zinc complexes (Table 3, entries 5–8), it is evident that **5** bearing Schiff-base ligands with 3,4,5-methoxy substituents is also the most effective catalyst in terms of rate, molecular weight and control. In general, polymers catalyzed by the zinc complexes **5–8** possessed very narrow distributions (PDI: 1.03–1.18), indicating less transesterification during the polymerization process [26]. Complex **5** bearing the 3,4,5-methoxy substituents exhibited better activity than did **6** with 2,4,6-methoxy substituents, **7** with 2,4-methoxy substituents and **8** without any methoxy substituents, as was seen for the organoaluminum complexes. These results strongly suggest that the use of 3,4,5-methoxy substituents in complexes of this type favors PCL formation.

During the preliminary experiments, the effect of temperature in the ROP of ϵ -CL at a fixed ratio of 250:1:1 ([ϵ -CL]:[catalyst]:[BnOH]) was investigated. At room temperature (25 °C), **1** exhibited no activity for the ROP of ϵ -CL (Table 3, entries 9). When the polymerization was performed at 50 °C over 18 h, the activity trend followed the order of **1** > **3** > **2** > **4** > **5** > **6** > **7** > **8** (Table 3, entries 10–17), which is similar to the trend observed at 100 °C. More specifically, **1** exhibited the best catalytic activity for the ROP of ϵ -CL, giving 99% conversion. In the case of aluminum, polymer molecular weights were higher at 50 °C and close to the calculated M_n than at 100 °C (e.g., see runs 1 and 10, Table 3), which suggests that the active species is approaching its thermal stability level at the higher temperature [27]. At 50 °C, only 18–30% of the monomer was converted to polymer over 18 h using the zinc complexes, i.e., the polymerization is much slower compared with 100 °C (Table 3, entries 14–17).

In order to gain more insight into the polymerization mechanism, **1** and **5** with differing amounts of benzyl alcohol were used as catalysts for the ROP of ϵ -CL. In the absence of benzyl alcohol, the polymerization of ϵ -CL catalyzed by **1** proceeded fastest, reaching 99% conversion in 35 min. at 100 °C (Table 3, entry 22). The resultant PCL had a larger M_n (76,000) than the theoretical M_n value, and a broad polydispersity (PDI = 2.75) indicative of a less controlled process likely due to backbiting or transesterification [28]. Increasing the ratio of [BnOH]:[catalyst]₀ from 1 to 2 and 4 decreased the polymerization rate. For example, in the presence of 4 equiv. of BnOH, a conversion of 99% was achieved over a longer polymerization time (120 min.). The results indicated that the addition of BnOH led to slower monomer conversion and decreased molecular weight (Table 3, entry 22–25). In the presence of 1 equiv. of BnOH, **1** exhibited similar activity to the system used in the absence of BnOH, whereas excess BnOH led to a decrease. This is thought to be due to decomposition of the catalyst [29]. For complex **5**, the absence of BnOH slowed the monomer conversion and poor control was noted (Table 3, entry 26). When the ratio of [BnOH]₀:[catalyst]₀ is 1, the conversion reached 51% after 2 h which is the best compared with other ratios and the system exhibited good control (PDI 1.03). The results

indicated BnOH is necessary in the zinc systems for enhanced control and acceleration of the polymerization process, however increasing the amount of BnOH proved detrimental to conversion, molecular weight and control (Table 3, entries 27–29).

Table 3. The ROP of ϵ -CL catalyzed by 1–8 ^a.

Entry	Complex	[CL]:[Cat]:[BnOH]	T (°C)	Time (min)	Conversion (%) ^b	M_n , calc (Da) ^c	M_n , GPC (Da) ^d	M_w , GPC (Da) ^d	M_w/M_n ^e
1	1	250:1:1	100	40	99	28,358	17,000	28,000	1.74
2	2	250:1:1	100	120	99	28,358	16,000	30,000	1.87
3	3	250:1:1	100	100	98	27,183	16,000	30,200	1.90
4	4	250:1:1	100	120	99	28,358	12,000	28,100	2.41
5	5	250:1:1	100	460	95	27,183	14,500	15,000	1.03
6	6	250:1:1	100	720	99	28,358	6700	7300	1.10
7	7	250:1:1	100	470	98	28,072	7100	8300	1.18
8	8	250:1:1	100	1560	95	27,183	7800	9100	1.18
9	1	250:1:1	25	720	4	-	-	-	-
10	1	250:1:1	50	1080	99	28,358	22,100	33,000	1.46
11	2	250:1:1	50	1080	90	25,790	20,000	39,000	1.96
12	3	250:1:1	50	1080	95	27,183	21,000	34,000	1.62
13	4	250:1:1	50	1080	85	24,363	20,237	39,000	1.93
14	5	250:1:1	50	1080	30	8669	5900	7000	1.20
15	6	250:1:1	50	1080	20	5821	3400	4400	1.28
16	7	250:1:1	50	1080	19	5530	3300	4300	1.29
17	8	250:1:1	50	1080	18	5821	5700	6800	1.20
18 ^f	1	250:1:1 ^f	100	720	99	28,358	9200	16,000	1.75
19 ^f	5	250:1:1 ^f	100	720	7	-	-	-	-
20	1	125:1:1	100	120	99	14,233	7300	11,300	1.56
21	1	500:1:1	100	120	99	56,716	24,000	49,400	2.04
22	1	250:1:0	100	35	99	28,250	76,000	210,000	2.75
23	1	250:1:1	100	40	99	28,358	17,000	28,000	1.74
24	1	250:1:2	100	115	99	14,233	6500	14,600	2.25
25	1	250:1:4	100	120	99	7200	3900	6200	1.60
26	5	250:1:0	100	120	40	28,250	25,500	62,500	2.45
27	5	250:1:1	100	120	51	27,183	14,500	15,000	1.03
28	5	250:1:2	100	120	26	8125	7800	10,500	1.34
29	5	250:1:4	100	120	13	4959	4000	5300	1.33

^a Polymerizations were carried out in toluene, [CL]₀ = 2 M. ^b Determined by ¹H NMR spectroscopy. ^c M_n , calc = ([CL]₀/[cat]₀) × Conv.% × 114.14; In the presence of BnOH, M_n , cal = 114.14 × ([CL]₀/[BnOH]₀) × conv. (%) + 108.13. ^d Obtained from GPC analysis and calibrated against the polystyrene standard, multiplied by 0.56. ^e Obtained from GPC analysis. ^f Reactions were carried out under air.

On the other hand, the ROP of **1** reached high conversion (99%) after 120 min. when the catalyst concentration was half ([CL]:[catalyst]:[BnOH] = 500:1:1) (Table 3, entry 21). As expected, the M_n values could be controlled by varying the CL:catalyst molar ratio (125:1, 250:1, 500:1) (Table 3, run 1, 20–21).

The air stability of these complexes were examined, **1** and **5** were used to initiate the polymerization of ϵ -CL at 100 °C with a [CL]:[catalyst]:[BnOH] ratio of 250:1:1 under air. Surprisingly, complex **1** successfully initiated the polymerization of ϵ -CL under air after 720 min. with a 99% conversion. However, **5** failed to initiate the polymerization under the same conditions (Table 3, entries 18–19). These results revealed that complex **1** can tolerate moisture during the polymerization process.

Kinetic studies were performed using 1–8. Plots of $\ln([CL]_0/[CL]_t)$ versus time are shown in Figure 3 (aluminum complexes 1–4) and Figure 4 (zinc complexes 5–8). Semilogarithmic plots obtained when using aluminum complexes are curves, which implied the polymerizations of ϵ -CL proceeded in two stages: the first is an induction period then followed by a first-order linear relationship dependence of monomer concentration (Figure 3). It is notable that all aluminum catalysts showed different induction periods dependent the type of catalysts. To clarify whether the induction period was caused by the presence of BnOH, the

ROP of ϵ -CL using **1** without BnOH was investigated. This significant induction period (approximately 20 min.) also existed in the absence of BnOH for complex **1** (Figure S15, Table 3, entry 22). These results suggest that the induction periods in the ROP of ϵ -CL were not caused by the coordination between aluminum complexes and BnOH when forming the active alkoxide species, but could be caused by the coordination between ϵ -CL and aluminum complexes [30]. The calculated slope of the linear section of the curve is equal to the apparent polymerization rate constant [31]. The aluminum complex **1** displayed the highest catalytic activity ($k_{\text{obs}} = 2562 \times 10^{-4} \text{ min}^{-1}$, $R = 0.9764$) compared to **3**, **2** and **4** ($k_{\text{obs}} = 1253 \times 10^{-4} \text{ min}^{-1}$, $R = 0.9924$; $k_{\text{obs}} = 903 \times 10^{-4} \text{ min}^{-1}$, $R = 0.9986$; $k_{\text{obs}} = 729 \times 10^{-4} \text{ min}^{-1}$, $R = 0.9973$, respectively).

The zinc systems (Figure 4) exhibited a near linear relationship, which implied that the polymerization followed a first-order dependence on the monomer concentration and the polymerization was controllable. Zinc complex **5** exhibited a better catalytic activity ($k_{\text{obs}} = 63 \times 10^{-4} \text{ min}^{-1}$) compared to **7** ($k_{\text{obs}} = 44 \times 10^{-4} \text{ min}^{-1}$), **6** ($k_{\text{obs}} = 19 \times 10^{-4} \text{ min}^{-1}$) and **8** ($k_{\text{obs}} = 17 \times 10^{-4} \text{ min}^{-1}$). The results showed that the catalytic activity of complexes for ϵ -CL decreased in the order of **1** (3,4,5-methoxy) > **3** (2,4-methoxy) > **2** (2,4,6-methoxy) > **4** (aniline) > **5** (3,4,5-methoxy) > **7** (2,4-methoxy) > **6** (2,4,6-methoxy) \geq **8** (aniline). Moreover, the k_{obs} difference between the aluminum complexes and zinc complexes indicates that metal center can dramatically affect the catalytic activity of ϵ -CL. Further, the substituent pattern of the methoxy groups on the Schiff-base ligands can strongly influence the polymerization rate for both the Al and Zn species, as well as the induction period for Al. For example, the k_{obs} value with the sequence of **1** (3,4,5-trimethoxy) > **3** (2,4-trimethoxy) > **2** (2,4,6-trimethoxy). In “Hammett” terms [32], the presence of two *meta*-methoxy groups (electron withdrawing) and a *para*-methoxy (electron donating) group as in **1** and **5**, enhances the ability of the metal to attack (nucleophilic) the carbonyl group of the caprolactone versus complexes possessing only *para*-/*ortho*-(**2**, **3**, **6** and **7**) or no methoxy substituents (**4** and **8**). The ^1H NMR results for the aluminum complexes verified the influence of the methoxy groups. As shown in the ^1H NMR spectra, chemical shifts assigned for the AlCH_3 group in **1–3** are -0.79 (**1**), -1.00 (**2**), -0.95 (**3**), respectively (Figure S1). The chemical shift order of **1** > **3** > **2** revealed that Lewis acidity of **1** is also larger than **3** and **2** [33]. This supports the polymerization activity trend. Lastly, the k_{obs} value of complex **4** (aniline) is smaller than **1** (3,4,5-trimethoxy) which suggests that ligands with electron donating groups on the Schiff-base ligand enhance the catalytic activity, which is in agreement with observations for *ortho*-OMe-substituted (salen)AlCl [34] and $[(\text{L}^4)\text{ZnEt}]_2$ ($\text{L}^4 = 2\text{-[1-[2-(dimethylamino)ethylimino]ethyl]-4-methoxyphenol}$) [35].

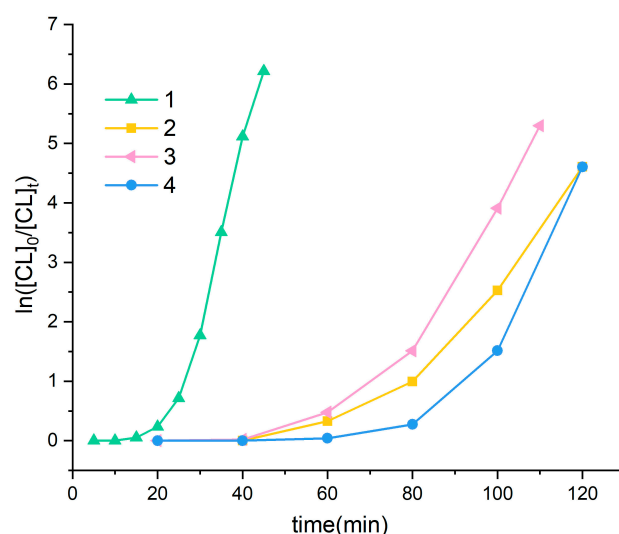


Figure 3. Plots of $\ln([\text{CL}]_0/[\text{CL}]_t)$ versus time catalyzed by organoaluminum complexes **1** (\blacktriangle), **2** (\blacksquare), **3** (\blacklozenge), **4** (\bullet); reaction conditions: $[\text{CL}]:[\text{catalyst}]:[\text{BnOH}] = 250:1:1$, $[\text{CL}] = 16.44 \text{ mmol}$, $[\text{BnOH}] = 0.01 \text{ M}$, reaction temperature: 100°C .

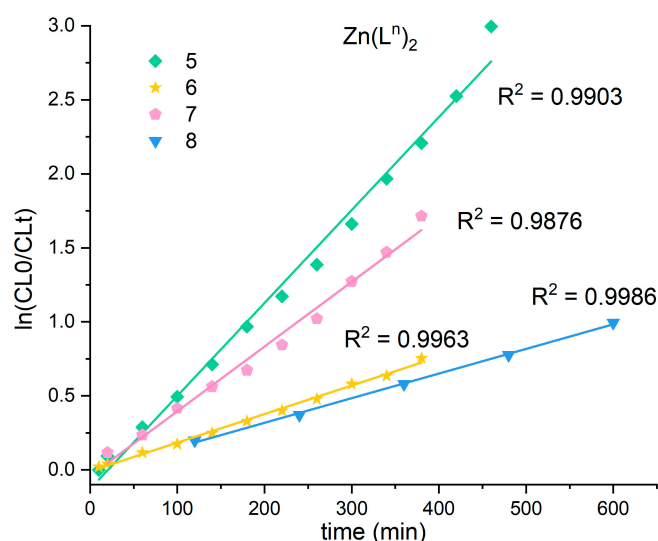


Figure 4. Plots of $\ln([CL]_0/[CL]_t)$ versus time catalyzed by zinc complexes **5** (◆), **6** (★), **7** (◆), **8** (▼); Reaction conditions: $[CL]:[catalyst]:[BnOH] = 250:1:1$, $[CL] = 16.44$ mmol, $[BnOH] = 0.01$ M, reaction temperature: 100°C .

End-group analysis was carried out using ^1H NMR spectroscopy and MALDI-TOF mass spectrometry (Figures 5 and 6). The ^1H NMR spectrum of the PCL produced by **1** (Table 3, entry 1) indicated the presence of one benzyl group (peaks k and m) and L^1 (peak g, f) group (Figure 5). The MALDI-TOF results of the same PCL (Table 3, entry 1) demonstrated there are two sets of main signals ascribed to the end groups with benzyl group and the L^1 moiety (Figure 6). One main set of peaks is $107.13 + 114.14n + 1.01 + 22.99$ attributed to $BnOH + (CL)_n + Na^+$. The other set of peaks is $398.52 + 114.14n + 1.01 + 68.97$ attributed to $L^1H + (CL)_n + 3Na^+$. The ^1H NMR spectroscopy and MALDI-TOF results suggest the existence of benzyl-capped PCL and L^1 -capped PCL, which implies that the polymerization proceeds via a coordination–insertion mechanism, where the monomer coordinates to the metal followed by the acyl oxygen bond cleavage of the monomer and chain propagation.

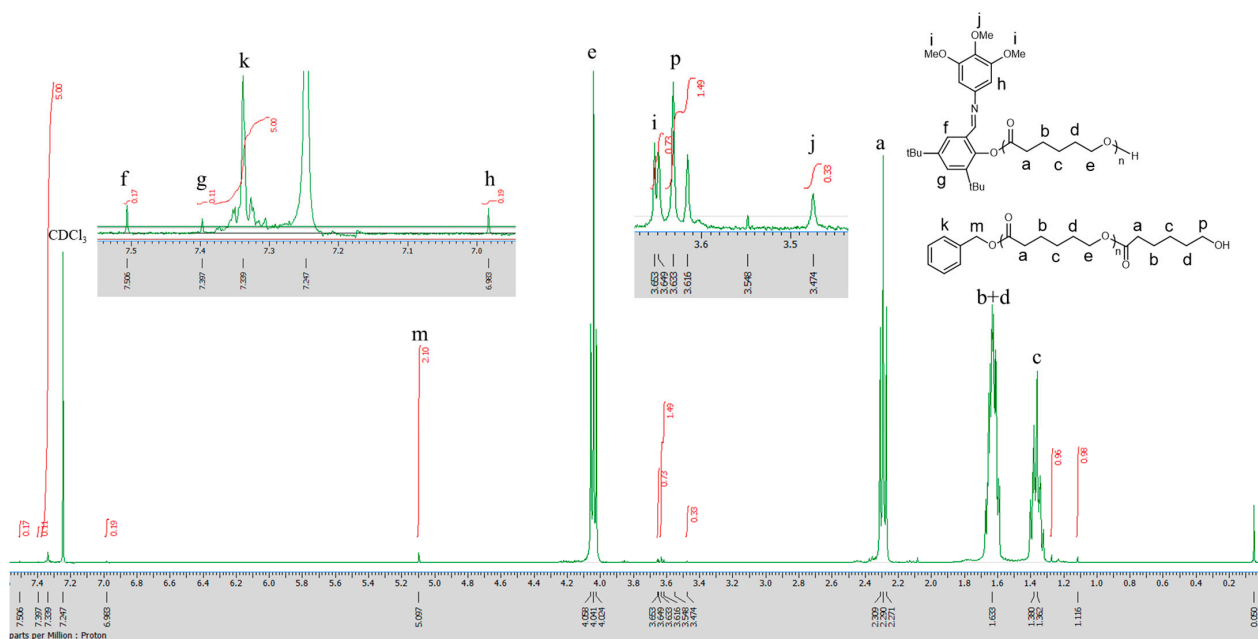


Figure 5. ^1H NMR spectrum of PCL initiated by complex **1** in the ratio of $[CL]:[catalyst]:[BnOH] = 250:1:1$ (CDCl_3 , 25°C , 400 MHz) (Table 3, entry 1).

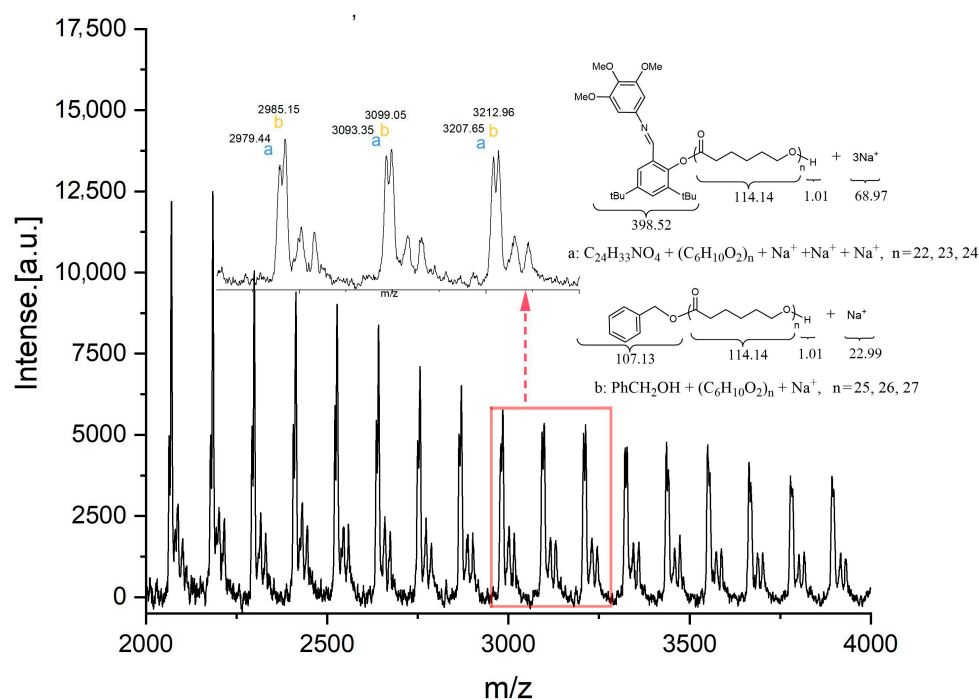


Figure 6. MALDI-TOF analysis for the PCL produced by complex 1 ([CL]:[catalyst]:[BnOH] = 250:1:1, 100 °C).

3.2. The ROP of Copolymer P(CL-co-GL) Catalyzed by the Aluminum Complexes

Given the better performance of complex 1, we applied this catalyst to the copolymerization of ϵ -CL and glycolide (GL), which is a copolymer that is widely used in industry [36–38]. The copolymerization reactions were conducted at 100 °C by adding the BnOH, ϵ -CL and glycolide (GL) together in the ratio [CL:GL]:[cat]:[BnOH] = [350:150]:[1]:[1] or [250:250]:[1]:[1]. The reaction was quenched with acidic methanol after 24 h. The microstructure and transesterification of the copolymer chain were demonstrated by ^1H NMR (DMSO- d_6) spectroscopic analysis, as shown in Figure 7.

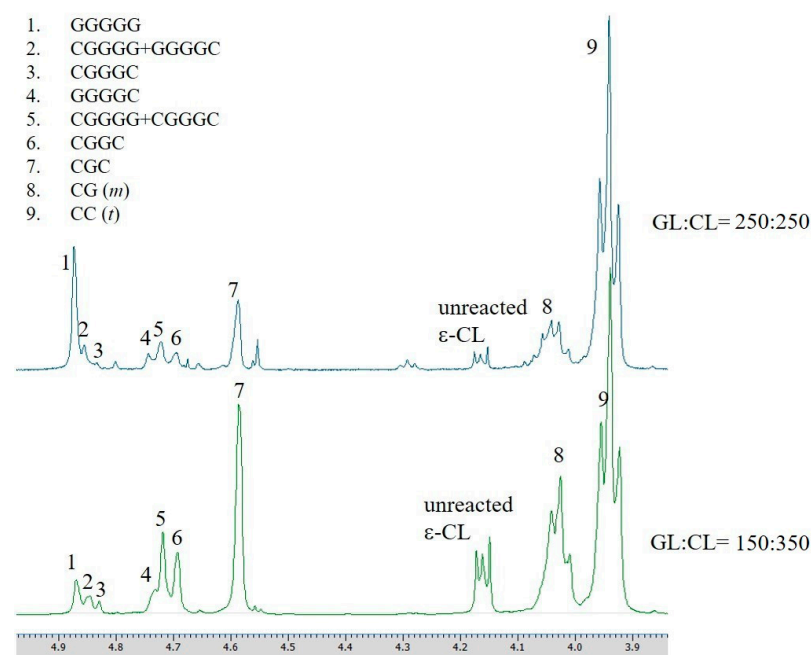


Figure 7. ^1H NMR spectroscopic analysis of the ϵ -CL/GL copolymer produced by complex 1.

The average lengths of caproyl and glycolidyl blocks (l_{CL}^e and l_{GL}^e) and R were calculated from the 1H NMR spectra, by using reported equations [39]. The average lengths depend on the composition ratio and monomers feed [40]. Ideally, the length of the glycolidyl block can be increased by increasing the feed of GL into the copolymer. However, the limited solubility of the GL derived copolymer in DMSO (100 °C), led to a lower content of glycolide than expected. The coefficient R represents the degree of randomness of the chain and if R is equal to 1, this indicates completely random chains, whereas if 0 then this indicates diblock copolymers [41]. The copolymer containing 30% of glycolidyl units is completely random with R is close to 1 (Table 4, entry 1), and the glycolidyl chain length is shorter than the caproyl one. When the content of glycolidyl is increased to 50% (Table 4, entry 2), higher l_{GL}^e , l_{CL}^e and lower R values were obtained which indicated a blockier structure and less transesterification. Therefore, **1** is a useful initiator for the copolymerization of ϵ -CL and GL, and the randomness of the sequences can be adjusted by the ratio of ϵ -CL and GL.

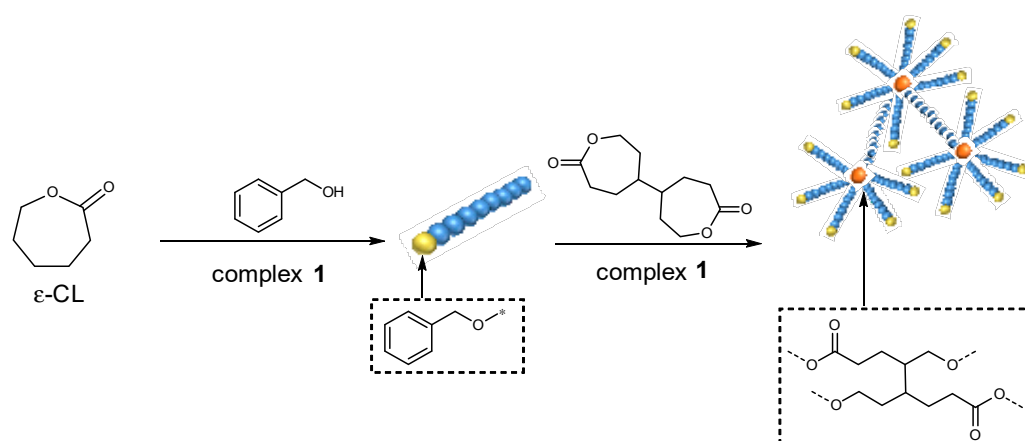
Table 4. Copolymerization of glycolide and ϵ -CL catalyzed by **1**^a.

Entry.	[GL]:[CL] (%)	Conversion (%) of GL ^b	Conversion (%) of CL ^b	l_{GL}^e ^c	l_{CL}^e ^c	R ^d	$M_{n, GPC}$ (Da) ^e	$M_{w, GPC}$ (Da) ^e	M_w/M_n ^f
1	150:350	97	86	0.79	2.97	0.96	19,900	59,400	2.99
2	250:250	98	97	1.31	5.73	0.58	8400	24,500	2.88

^a Polymerization conditions: catalyst = 0.066 mmol; BnOH = 0.065 (0.01 M in toluene); T = 100 °C. ^b obtained by 1H NMR spectroscopy; ^c average length of glycolidyl (GL) and caprolactone (CL) blocks in completely random chains; calculated from 1H NMR (DMSO-*d*6). ^d R , degree of randomness. ^e obtained from GPC analysis and calibrated against the polystyrene standard, multiplied by 0.56. ^f Obtained from GPC analysis.

3.3. The ROP of Cross-Linked PCL Catalyzed by the Aluminum Complexes

Core cross-linked poly(CL-*co*-BOD) polymers (BOD = 4,4'-bioxepane-7,7'-dione) were synthesized via a two-step method (Scheme 2). In the first step, ϵ -CL was polymerized in the presence of complex **1** and the initiator benzyl alcohol in the ratio 250:1:1 (100 °C) to produce living linear PCL arms. On completion of the first step (conversion = 99%, 1 h), BOD and **1** in toluene were added to the reaction solution (CL/BOD = 250:25 = 10). The BOD is a cross-linking component, which produces the core structure under ROP conditions. The molecular structure of poly(CL-*co*-BOD) was confirmed by 1H NMR (Figure 8). The BnOH end group, BOD and ϵ -CL peaks in the copolymer were evident in Figure 8, however, it proved difficult to calculate the BOD conversion given that peaks due to polyBOD and PCL were indistinguishable [42]. The mole ratio of CL:BOD monomer is 19.55 (verified by the integral peak area) which indicated that nearly half the BOD monomer are either pendant or unreacted in the poly(CL-*co*-BOD) core. We assume here that conversion of BOD is 51% according to the remaining BOD monomer. Analysis by GPC of the cross-linked polymer showed that the poly(CL-*co*-BOD) (Table 5, entry 1 and Figure S14) exhibited high M_n = 308,000, which is much larger than PCL (M_n = 17,000) (Table 5, entry 2), and narrow PDI = 1.71. The data suggested that complex **1** can be used to synthesize cross-linked PCL with high M_n .



Scheme 2. Synthesis of core cross-linked polymer via ring-opening polymerization.

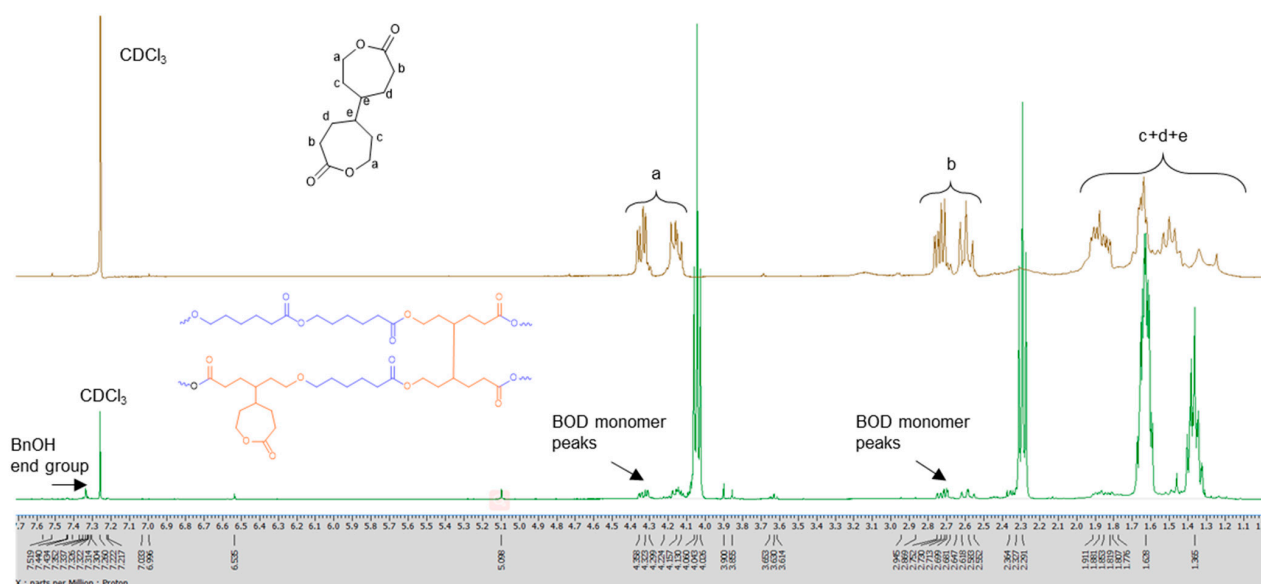


Figure 8. ^1H NMR (CDCl_3 , 400 MHz) analysis for BOD monomer (top) and cross-linked poly(CL-co-BOD) (bottom) produced by **1** ($[\text{CL}]:[\text{BOD}]:[\text{catalyst}]:[\text{BnOH}] = 250:25:1:1$, 100°C).

Table 5. Polymerization data for poly(CL-co-BOD) catalyzed by **1**^a.

Entry.	$[\text{CL}]:[\text{BOD}]$	Conversion (%) of CL ^b	Conversion (%) of BOD ^b	$M_{n,\text{GPC}}$ (Da) ^c	$M_{w,\text{GPC}}$ (Da) ^c	M_w/M_n ^d
1	250:250	99	51	308,000	526,000	1.71
2	250:0	99	-	17,000	28,000	1.74

^a Polymerizations were carried out in toluene, $[\text{CL}]_0 = 2\text{ M}$. ^b Determined by ^1H NMR spectroscopy. ^c $M_n, \text{calcd} = ([\text{CL}]_0/[\text{cat}]_0) \times \text{Conv.}\% \times 114.14$. ^d Obtained from GPC analysis and calibrated against the polystyrene standard, multiplied by 0.56. ^e Obtained from GPC analysis.

4. Materials and Methods

The preparation of the aluminum or zinc complexes and the ring opening polymerizations were carried out under an inert atmosphere of dry nitrogen by using Schlenk systems, cannula techniques or a glove box. Toluene (Aldrich, Dorset, UK) was refluxed over Na-benzophenone/Ketyl (Aldrich, Dorset, UK), acetonitrile (Aldrich, Dorset, UK) was refluxed over calcium hydride (Aldrich, Dorset, UK), whilst benzyl alcohol (Aldrich, Dorset, UK) was dried over molecular sieves. ϵ -CL (Aldrich, Dorset, UK) and 2,4-dimethoxyaniline (Alpha Aesar, Lancashire, UK) were dried over calcium hydride, and were distilled prior to use. The purity of the monomers ϵ -CL and GL were determined to be 99.6 and 99.5 %, respectively.

respectively (determined by ^1H NMR spectroscopy, JEOL ECZ 400S spectrometer, Tokyo, Japan). 3,5-Di-*tert*-butyl-2-hydroxybenzaldehyde (Matrix Scientific, Columbia, SC, U.S.A.), 3,4,5-trimethoxyaniline (Alpha Aesar, Tewksbury, MA, U.S.A.), diethylzinc (ZnEt_2) (0.9 M in hexane) (Acros Organics, Loughborough, UK), trimethylaluminum (AlMe_3) (2.0 M in toluene) (Aldrich, Dorset, UK) were purchased from commercial sources and used directly. 2,4,6-Trimethoxyaniline and Complex **5** was prepared by the reported procedure [25]. NMR spectra were recorded at 400.2 MHz on a JEOL ECZ 400S spectrometer (JEOL Ltd., Tokyo, Japan) with TMS $\delta\text{H} = 0$ as the internal standard or residual protic solvent [CD_3CN , $\delta\text{H} = 1.94$]. Chemical shifts are given in ppm (δ) and coupling constants (J) are given in Hertz (Hz). Elemental analyses were performed by the elemental analysis service at the Department of Chemistry, the University of Hull or OEA labs Ltd. FTIR spectra (nujol mulls, KBr windows) were recorded on a Nicolet Avatar 360 FT-IR spectrometer (Thermo Nicolet Corporation., Madison, WI, U.S.A.). MALDI-TOF mass spectra (Bruck, Hull, UK) were acquired by averaging at least 100 laser shots. Molecular weights were calculated from the experimental traces using the OmniSEC 467 (Thermo Nicolet Corporation., Madison, WI, U.S.A.).

4.1. Synthesis of 2,4-Di-*Tert*-Butyl-6-(((3,4,5-Trimethoxyphenyl)Imino)Methyl)Phenol (L^1H)

L^1H was prepared according to a procedure described previously for related Schiff bases [21,22,43]. 3,5-di-*tert*-butyl-2-hydroxybenzaldehyde (3.51 g, 15.00 mmol) was mixed with 3,4,5-trimethoxyaniline (2.75 g, 15.03 mmol) in refluxing ethanol (200 mL). A yellow crystalline solid separated slowly upon stirring. The resulting mixture was stirred for 4 h and the solid was isolated by filtration then washed with ice-cold methanol (30 mL). The solid was further recrystallized from dichloromethane (10 mL)/methanol (30 mL). Yield: 54% (3.23 g). ^1H NMR (400 MHz, CD_3CN , 25 °C): δ 8.84 (s, 1H, $\text{CH}=\text{N}$), 7.48–7.49 (d, $J = 2$ Hz, 1H, ArH), 7.42–7.43 (m, 1H, ArH), 6.72 (s, 2H, ArH), 3.87 (s, 6H, CH_3), 3.73 (s, 3H, CH_3), 1.45 (s, 9H, *t*Bu), 1.33 (s, 9H, *t*Bu). IR (KBr disc, cm^{-1}): 2950 ($\nu_{\text{Ph-H}}$), 1615 ($\nu_{\text{C}=\text{N}}$), 1228 ($\nu_{\text{C-O}}$).

4.2. Synthesis of 2,4-Di-*Tert*-Butyl-6-(((2,4,6-Trimethoxyphenyl)Imino)Methyl)Phenol (L^2H)

L^2H was prepared using a procedure similar to that described for L^1H . 3,5-di-*tert*-butyl-2-hydroxybenzaldehyde (3.51 g, 15.00 mmol) was mixed with 2,4,6-trimethoxyaniline (2.75 g, 15.01 mmol) in refluxing ethanol (200 mL). An orange crystalline solid separated slowly upon stirring. The resulting mixture was stirred for 4 h and the solid was isolated by filtration then washed with ice-cold methanol (30 mL). The solid was further recrystallized from dichloromethane (10 mL)/methanol (30 mL). Yield: 70% (4.19 g). ^1H NMR (400 MHz, CD_3CN , 25 °C): δ 9.16 (s, 1H, $\text{CH}=\text{N}$), 7.41, 7.40 (d, $J = 2.5$, 1H, ArH), 7.29, 7.28 (t, $J = 1.9$ Hz, 1H, 1H, ArH), 6.32 (s, 2H, ArH), 3.88 (s, 6H, OCH_3), 3.84 (s, 3H, OCH_3), 1.45 (s, 9H, *t*Bu), 1.32 (s, 9H, *t*Bu). IR (KBr disc, cm^{-1}): 1611 ($\nu_{\text{C}=\text{N}}$), 1230 ($\nu_{\text{C-O}}$).

4.3. Synthesis of 2,4-Di-*Tert*-Butyl-6-(((2,4-Trimethoxyphenyl)Imino)Methyl)Phenol (L^3H)

L^3H was prepared using a procedure similar to that described for L^1H . 3,5-di-*tert*-butyl-2-hydroxybenzaldehyde (5.80 g, 24.78 mmol) was mixed with 2,4-dimethoxyaniline (3.80 g, 24.78 mmol) in refluxing ethanol (200 mL). An orange crystalline solid separated slowly upon stirring. The resulting mixture was stirred for 4 h and the solid was isolated by filtration then washed with ice cold methanol (30 mL). The solid was further recrystallized from dichloromethane (10 mL)/methanol (30 mL). Yield: 33% (3.00 g). ^1H NMR (400 MHz, CD_3CN , 25 °C): δ 8.78 (s, 1H, $\text{CH}=\text{N}$), 7.42 (d, $J = 2.5$ Hz, 1H, ArH), 7.34 (d, $J = 2.5$ Hz, 1H, ArH), 7.29 (d, $J = 8.7$ Hz, 1H, ArH), 6.62 (d, $J = 2.7$ Hz, 1H, ArH), 6.57 (dd, $J = 8.7, 2.7$ Hz, 1H, ArH), 3.87 (s, 3H, OCH_3), 3.80 (s, 3H, OCH_3), 1.42 (s, 9H, *t*Bu), 1.29 (s, 9H, *t*Bu). IR (KBr disc, cm^{-1}): 1616 ($\nu_{\text{C}=\text{N}}$), 1250 ($\nu_{\text{C-O}}$).

4.4. Synthesis of 2,4-Di-*Tert*-Butyl-6-((Phenylimino)Methyl)Phenol (L^4H)

L^2H was prepared using a procedure similar to that described for L^1H . 3,5-di-*tert*-butyl-2-hydroxybenzaldehyde (11.71 g, 50.00 mmol) was mixed with aniline (4.65 mL,

50.00 mmol) in refluxing ethanol (200 mL). An orange crystalline solid separated slowly upon stirring. The resulting mixture was stirred for 4 h and the solid was isolated by filtration then washed with ice cold methanol (30 mL). The solid was further recrystallized from dichloromethane (10 mL)/methanol (30 mL). Yield: 80% (12.38 g). ^1H NMR (400 MHz, CD_3CN , 25 °C): δ 8.81 (s, 1H, $\text{CH}=\text{N}$), 7.50–7.29 (m, 7H, ArH), 1.45 (s, 9H, *t*Bu), 1.33 (s, 9H, *t*Bu). IR (KBr disc, cm^{-1}): 3174 (ν_{OH}), 3062 ($\nu_{\text{Ph-H}}$), 1618 ($\nu_{\text{C}=\text{N}}$), 1250 ($\nu_{\text{C-O}}$).

4.5. Synthesis of $[\text{Al}(\text{L}^1)(\text{Me})_2]$ (**1**)

In a 25 mL Schlenk tube under nitrogen, L^1H (0.27 g, 0.68 mmol) was dissolved in dry toluene (20 mL), one equivalent of AlMe_3 (0.35 mL, 0.68 mmol) was added dropwise into the reaction solution. The system was refluxed for 12 h, and following removal of volatiles in vacuo, the residue was extracted in warm MeCN (15 mL), affording on prolonged standing in the refrigerator (5 °C) small, yellow crystals. Yield 52% (0.14 g). Anal. Calcd for $\text{C}_{26}\text{H}_{38}\text{NO}_4\text{Al}$ (455.55 g mol^{-1}): C, 68.55; H, 8.41; N, 3.07%; Found: C, 67.79; H, 8.22; N, 3.42%. HR-MS (EI): m/z 457.24 $[\text{Al}(\text{L}^1)(\text{Me})_2 + \text{H}]^+$, 400.31 $[\text{Al}(\text{L}^1)(\text{Me})_2 - \text{Al}(\text{Me})_2 + \text{H}]^+$. ^1H NMR (400 MHz, CD_3CN , 25 °C): δ 8.82 (s, 1H, $\text{CH}=\text{N}$), 7.58–7.59 (d, $J = 2.8$, 1H, ArH), 7.36–7.35 (m, $J = 2.8$, 1Hc, ArH), 6.70 (s, 2H, ArH), 3.82 (s, 6H, CH_3), 3.72 (s, 3H, CH_3), 1.41 (s, 9H, *t*Bu), 1.33 (s, 9H, *t*Bu), -0.79 (s, 6H, AlMe_2). IR (KBr disc, cm^{-1}): 1613 ($\nu_{\text{C}=\text{N}}$), 1237 ($\nu_{\text{C-O}}$), 708 ($\nu_{\text{Al-O}}$), 587 ($\nu_{\text{Al-N}}$), 609 ($\nu_{\text{Al-C}}$).

4.6. Synthesis of $[\text{Al}(\text{L}^2)(\text{Me})_2]$ (**2**)

The synthesis of **2** was carried out according to the same procedure as for **1**, but using L^2H . Yield 34% (0.093 g). Anal. Calcd for $\text{C}_{26}\text{H}_{38}\text{NO}_4\text{Al}$ (455.55 g mol^{-1}): C, 68.55; H, 8.41; N, 3.07%; Found: C, 67.94; H, 8.36; N, 3.11%. HR-MS (EI): m/z 400.27 $[\text{Al}(\text{L}^2)(\text{Me})_2 - \text{Al}(\text{Me})_2 + \text{H}]^+$. ^1H NMR (400 MHz, CD_3CN , 25 °C): δ 8.58 (s, 1H, $\text{CH}=\text{N}$), 7.57–7.58 (d, $J = 2.4$, 1H, ArH), 7.22–7.21 (d, $J = 2.8$, 1Hc, ArH), 6.34 (s, 2H, ArH), 3.82 (s, 6H, OCH_3), 3.86 (s, 3H, OCH_3), 1.41 (s, 9H, *t*Bu), 1.30 (s, 9H, *t*Bu), -1.00 (s, 6H, AlMe_2). IR (KBr disc, cm^{-1}): 1614 ($\nu_{\text{C}=\text{N}}$), 1230 ($\nu_{\text{C-O}}$), 705 ($\nu_{\text{Al-O}}$), 575 ($\nu_{\text{Al-N}}$), 604 ($\nu_{\text{Al-C}}$).

4.7. Synthesis of $[\text{Al}(\text{L}^3)(\text{Me})_2]$ (**3**)

The synthesis of **3** was carried out according to the same procedure as for **1**, but using L^3H . Yield 40% (0.15 g). Anal. Calcd for $\text{C}_{25}\text{H}_{36}\text{NO}_3\text{Al}$ (425.55 g mol^{-1}): C, 70.56; H, 8.53; N, 3.29%; Found: C, 68.83; H, 8.21; N, 3.27%. * HR-MS (EI): m/z 427.30 $[\text{Al}(\text{L}^3)(\text{Me})_2 + \text{H}]^+$, 370.24 $[\text{Al}(\text{L}^3)(\text{Me})_2 - \text{Al}(\text{Me})_2 + \text{H}]^+$. ^1H -NMR (400 MHz, CD_3CN , 25 °C): δ 8.58 (s, 1H, $\text{CH}=\text{N}$), 7.57 (d, $J = 2.5$ Hz, 1H, ArH), 7.33 (d, $J = 2.8$ Hz, 1H, ArH), 7.28 (d, $J = 8.7$ Hz, 1H, ArH), 6.63 (t, $J = 8.4$ Hz, 2H, ArH), 3.89 (s, 3H, OCH_3), 3.84 (s, 3H, OCH_3), 1.41 (s, 9H, *t*Bu), 1.31 (s, 9H, *t*Bu), -0.93 (s, 6H, AlMe_2). IR (KBr disc, cm^{-1}): 1615 ($\nu_{\text{C}=\text{N}}$), 1240 ($\nu_{\text{C-O}}$), 755 ($\nu_{\text{Al-O}}$), 579 ($\nu_{\text{Al-N}}$), 676 ($\nu_{\text{Al-C}}$). * Despite repeated attempts, the %C was also low.

4.8. Synthesis of $[\text{Al}(\text{L}^4)(\text{Me})_2]$ (**4**)

The synthesis of **4** was carried out following the previous report [25]. A mixture of L^4H (3.68 g, 11.89 mmol) and AlMe_3 (6 mL, 12.00 mmol) in toluene (20 mL) was stirred for 12 h at 150 °C. Volatile materials were removed under vacuum to give yellow needle crystals, and then acetonitrile (20 mL) was transferred to the suspension. A yellow crystalline solid was obtained after filtering and prolonged standing at 0 °C. Yield 78% (3.37 g). HR-MS (EI): m/z 367.28 $[\text{Al}(\text{L}^4)(\text{Me})_2 + \text{H}]^+$, 310.22 $[\text{Al}(\text{L}^4)(\text{Me})_2 - \text{Al}(\text{Me})_2 + \text{H}]^+$. ^1H NMR (400 MHz, CD_3CN , 25 °C): δ 8.52 (s, 1H, $\text{CH}=\text{N}$), 7.59–7.60 (d, $J = 2.4$ Hz, 1H, ArH), 7.26–7.51 (m, 6H, ArH), 1.43 (s, 9H, *t*Bu), 1.40 (s, 9H, *t*Bu), -1.16 (s, 6H, AlMe_2). IR (KBr disc, cm^{-1}): 1614 ($\nu_{\text{C}=\text{N}}$), 1230 ($\nu_{\text{C-O}}$), 705 ($\nu_{\text{Al-O}}$), 575 ($\nu_{\text{Al-N}}$), 604 ($\nu_{\text{Al-C}}$).

4.9. Synthesis of $[\text{Zn}(\text{L}^1)_2] \cdot 2\text{CH}_3\text{CN}$ (**5**)

Synthesis of **5** was carried out according to the same procedure as **1**, but using diethyl zinc. Yield 48% (0.13 g). Anal. Calcd for $\text{C}_{52}\text{H}_{70}\text{N}_4\text{O}_8\text{Zn}$ (944.53 g mol^{-1}): C, 66.13; H, 7.47; N, 5.93%; Found: C, 66.35; H, 8.05; N, 5.30%. HR-MS (EI): m/z 370.34 $[\text{Zn}(\text{L}^1)_2 - \text{Zn}(\text{L}^1) -$

(Me)₂ + H]⁺, 400.29 [Zn(L¹)₂ − (Zn(L¹)) + H]⁺. ¹H NMR (400 MHz, CD₃CN, 25 °C): δ 8.65 (s, 2H, CH=N), 7.51–7.50 (d, J = 2.4, 2H, ArH), 7.26–7.27 (d, J = 2.4, 2H, ArH), 6.44 (s, 4H, ArH), 3.62 (s, 6H, OCH₃), 3.46 (s, 12H, OCH₃), 1.38 (s, 18H, *t*Bu), 1.32 (s, 18H, *t*Bu). IR (KBr disc, cm^{−1}): 1612 (ν C=N), 1237 (ν C–O–), 661 (ν Zn–O), 598 (ν Zn–N).

4.10. Synthesis of [Zn(L²)₂] (6)

The synthesis of **6** was carried out according to the same procedure as **5**, but using L²H. Yield 40% (0.11 g). Anal. Calcd for C₄₈H₆₄N₂O₈Zn (862.43 g mol^{−1}): C, 66.85; H, 7.48; N, 3.25%. Found: C, 66.61; H, 7.52; N, 3.94%. HR-MS (EI): ^{m/z} 400.26 [Zn(L²)₂ − (Zn(L²)) + H]⁺. ¹H NMR (400 MHz, CD₃CN, 25 °C): δ 8.36 (s, 2H, CH=N), 7.39–7.38 (d, J = 2.8 Hz, 2H, ArH), 6.96–6.95 (d, J = 2.8, 2H, ArH), 6.00 (s, 4H, ArH), 3.74 (s, 6H, OCH₃), 3.52 (s, 12H, OCH₃), 1.33 (s, 18H, *t*Bu), 1.28 (s, 18H, *t*Bu). IR (KBr disc, cm^{−1}): 1614 (ν C=N), 1227 (ν C–O–), 687 (ν Zn–O), 571 (ν Zn–N).

4.11. Synthesis of [Zn(L³)₂] (7)

Synthesis of **7** was carried out according to the same procedure as **5**, but using L³H as ligand to react with diethyl zinc. Yield 60% (0.20 g). Anal. Calcd for C₄₆H₆₀N₂O₆Zn (802.37 g mol^{−1}): C, 68.86; H, 7.54; N, 3.49%. Found: C, 68.71; H, 7.88; N, 3.75%. HR-MS (EI): ^{m/z} 801.41 [Zn(L³)₂ + H]⁺. ¹H NMR (400 MHz, CD₃CN, 25 °C): δ 8.50 (s, 2H, CH=N), 7.32–7.33 (d, J = 2.8 Hz, 2H, ArH), 7.11–7.13 (q, J = 2.9 Hz, 4H, ArH), 6.44–6.47 (dd, J = 8.7 Hz, 2H, ArH), 6.37–6.38 (d, J = 2.5 Hz, 2H, ArH), 3.72 (s, 6H, OCH₃), 3.37 (s, 6H, OCH₃), 1.26 (s, 18H, *t*Bu), 1.14 (s, 18H, *t*Bu). IR (KBr disc, cm^{−1}): 1616 (ν C=N), 1258 (ν C–O–).

4.12. Synthesis of [Zn(L⁴)₂] (8)

Synthesis of **8** was carried out according to the same procedure as **5**, but using L⁴H. Yield 75% (0.45 g). Anal. Calcd for C₄₂H₅₂N₂O₂Zn (682.27 g mol^{−1}): C, 73.94; H, 7.68; N, 4.11%. Found: C, 73.60; H, 7.62; N, 3.82%. HR-MS (EI): ^{m/z} 310.23 [Zn(L⁴)₂ − (Zn(L₂)) + H]⁺. ¹H NMR (400 MHz, CD₃CN, 25 °C): δ 8.58 (s, 2H, CH=N), 7.49 (d, J = 6.4 Hz, 2H, ArH), 7.29–7.15 (m, 12H, ArH), 1.34 (s, 18H, *t*Bu), 1.28 (s, 18H, *t*Bu). IR (KBr disc, cm^{−1}): 1612 (ν C=N), 1254 (ν C–O–), 744 (ν Zn–O).

4.13. ROP of ε-Caprolactone (ε-CL)

All polymerizations were carried out in Schlenk tubes under nitrogen atmosphere. ε-CL was polymerized using complexes **1–8** in the presence of BnOH (0.1 M in toluene) as a co-initiator. Complexes were weighed out in the glove box and then initiator and monomer were added to the flask successively via syringe. The molar ratio of monomer/catalyst/BnOH ([CL]/[Cat]/[BnOH]) is presented in Table 3. The reaction mixture was then placed into an oil bath preheated to the required temperature. The reaction was quenched by the addition of an excess of glacial acetic acid (0.2 mL), then the reaction solution was then poured into cold methanol (20 mL). The reaction conversion was monitored by ¹H NMR (400 MHz, CDCl₃, 25 °C) spectroscopic studies. The resulting polymer was washed several times with methanol, collected on filter paper and then dried under vacuum to constant weight at 40 °C. GPC (in THF) were used to determine molecular weights (*M*_n and PDI) of the polymer products.

4.14. ROP of Copolymerization of ε-Caprolactone (ε-CL) and Glycolide (GL)

All polymerizations were carried out in Schlenk tubes under nitrogen atmosphere. ε-CL and GL were polymerized using complexes **1** (0.03 g) in the presence of BnOH (6.58 mL) (0.1 M in toluene) as a co-initiator. The reaction mixture was then placed into an oil bath preheated to the required temperature 100 °C. The reaction was quenched by the addition of an excess of glacial acetic acid (0.2 mL), then the reaction solution was then poured into cold methanol (20 mL). The precipitated polymers were recovered by filtration, washed with methanol and dried at 60 °C overnight in a vacuum oven.

4.15. Polymerization Kinetics

Kinetic experiments were carried out following the previous polymerization method. At regular time intervals, 0.05 mL aliquots were removed, quenched with wet CDCl_3 (1 mL), and analyzed by ^1H NMR spectroscopy.

4.16. 4,4'-Bioxepane-7,7'-Dione (BOD) Cross Linker

4,4'-Bioxepane-7,7'-dione (BOD) was synthesized according to the literature [44]. A solution of 20.0 g of urea hydrogen peroxide in 100 mL of formic acid (99%) was stirred at room temperature for 2 h. The flask was immersed in an ice bath to control the exotherm resulting from the former procedure. Then, 10 g of 4,4'-bicyclohexanone was slowly added over 5–10 min with stirring while the ice bath was changed periodically. After 4 h, 200 mL of water was added to the mixture followed by extraction with chloroform (4 times 100 mL), after which the organic fractions were collected, washed with a saturated aqueous of sodium bicarbonate solution and dried overnight with sodium sulfate. The combined organic fractions were concentrated and dried under reduced pressure to yield a white powder (3.07, 27%). ^1H NMR (400 MHz, CDCl_3 , 25 °C): δ 4.35–4.28 (m, 2H), 4.19–4.11 (m, 2H), 2.75–2.66 (m, 2H), 2.61–2.54 (dd, J = 14.1, 12.5 Hz, 2H), 1.90–1.80 (m, 4H), 1.67–1.66 (m, 4H), 1.54–1.42 (m, 2H).

4.17. X-ray Crystallography

In all cases, crystals suitable for an X-ray diffraction study were grown from a saturated MeCN solution at 0 °C. All (except 7) single crystal X-ray diffraction data were collected at the UK National Crystallography service using Rigaku Oxford Diffraction ultra-high intensity instruments employing modern areas detectors. In all cases, standard procedures were employed for integration and processing of data. Data for 7 was collected at Hull on a Stoe IPDS2 image plate diffractometer operating with Mo $\text{K}\alpha$ radiation. Data were integrated and reduced using Stoe X-RED software.

Crystal structures were solved using dual space methods implemented within SHELXT [45]. Completion of structures was achieved by performing least squares refinement against all unique F^2 values using SHELXL-2018 [46]. Cambridge Crystallographic Data Centre (CCDC) numbers 2094365-69 and 2,099,692 contain the supplementary crystallographic data.

5. Conclusions

We have carried out a comparative study of the effect of methoxy substituents (2,4-, 2,4,6- and 3,4,5-patterns versus no methoxy substituents) at the aniline derived ring in a series of Schiff-base organoaluminum and zinc complexes. In the series $[\text{Al}(\text{L}^n)(\text{Me})_2]$, for the ROP of ϵ -CL in the presence (or absence) of BnOH, all complexes exhibited an induction period of up to 20 min., and there after the results indicated that ligands derived from anilines bearing 3,4,5-methoxy substituents favored the ROP process in terms of rate (with 1st order kinetics), molecular weight and control. The 3,4,5-methoxy containing system was also capable of the efficient ROP of ϵ -CL under air. The same complex was also capable of the copolymerization of ϵ -CL and glycolide (GL), as well as forming cross-linked PCL in the presence of 4,4'-bioxepane-7,7'-dione. In the case of the $[\text{Zn}(\text{L}^n)_2]$ series, results again indicated that the system bearing the 3,4,5-methoxy motif most greatly favored the ROP process. The zinc complexes did not exhibit an induction period and all performed the ROP with 1st order kinetics. The aluminum systems outperformed (in terms of rate) the zinc systems.

Supplementary Materials: The following are available online at <https://www.mdpi.com/article/10.3390/catal11091090/s1>: ^1H NMR spectra of 1–3 and 5–7; FTIR of 1–8 and L^{1-3}H ; GPC of poly(CL-co-BOD); Plot of $\ln[\text{CL}]_0/[\text{CL}]_t$ vs. t , $[\epsilon\text{-CL}]:[1]:[\text{BnOH}]$. Figure S1. ^1H NMR spectrum of (400 MHz, CD_3CN) spectra of 1–3. Figure S2. ^1H NMR spectrum of (400 MHz, CD_3CN) spectra of 5–7. Figure S3. FTIR of complex 1. Figure S4. FTIR of complex 2. Figure S5. FTIR of complex 3. Figure S6. FTIR

of complex 4. Figure S7. FTIR of complex 5. Figure S8. FTIR of complex 6. Figure S9. FTIR of complex 7. Figure S10. FTIR of complex 8. Figure S11. FTIR of complex L¹H. Figure S12. FTIR of complex L²H. Figure S13. FTIR of complex L³H. Figure S14. Gel permeation chromatography for poly(CL-co-BOD). Figure S15. Plot of $\ln[CL]_0/[CL]_t$ vs. t , $[-CL]:[1]:[BnOH] = 250:1:0$, at 100 °C according to the conditions in Table 3, entry 22.

Author Contributions: Conceptualization, C.R. and X.Z.; methodology, C.R. and X.Z.; formal analysis, C.R. and X.Z.; investigation, C.R. and X.Z.; ligand resources, T.A.N., M.C. and K.G., C.R. and X.Z.; writing—original draft preparation, C.R. and X.Z.; writing—review and editing, C.R. and X.Z.; supervision, C.R.; Crystallography K.C. and T.J.P.; project administration, C.R.; funding acquisition, C.R. All authors have read and agreed to the published version of the manuscript.

Funding: This research was funded by UKRI Creative Circular Plastic grant (EP/S025537/1).

Acknowledgments: X.Z. thanks the University of Hull for a Ph.D. scholarship. C.R. thanks the EPSRC for funding a PRIF grant (Evolving a Circular Plastics Economy grant EP/S025537/1). The EPSRC National Crystallographic Service Centre at Southampton is thanked for data. M.C. thanks the University of North Carolina for the award of an Undergraduate Research Assistantship.

Conflicts of Interest: There are no conflicts of interest to declare.

Appendix A

Table 1. Crystallographic data and refinement details for compounds 1–3, 5–7.

Compound	1	2	3	5	6	7
Empirical formula	C ₂₆ H ₃₈ NO ₄ Al	C ₂₆ H ₃₈ NO ₄ Al	C ₂₅ H ₃₆ NO ₃ Al	C ₅₂ H ₇₀ N ₄ O ₈ Zn	C ₄₈ H ₆₄ N ₂ O ₈ Zn	C ₄₈ H ₆₀ N ₂ O ₆ Zn
Formula weight	455.55	455.55	425.53	944.49	862.40	802.33
Crystal system	Tetragonal	Triclinic	Monoclinic	Orthorhombic	Monoclinic	Monoclinic
Temp (K)	100(2)	100(2)	100(2)	100(2)	100(2)	150(2)
Wavelength/Å	1.54178	0.71075	1.54178	0.71075	1.54178	0.71073
Space group	<i>P</i> 4 ₂ / <i>n</i>	<i>P</i> -1	<i>P</i> 2 ₁ / <i>c</i>	<i>Pbca</i>	<i>I</i> 2/ <i>a</i>	<i>P</i> 2 ₁ / <i>n</i>
<i>a</i> /Å	28.9022(5)	8.77450(10)	10.49237(5)	16.8034(4)	13.0291(4)	13.3203(9)
<i>b</i> /Å	28.9022(5)	11.85330(10)	20.94049(12)	20.9651(5)	27.0249(8)	10.1701(4)
<i>c</i> /Å	6.0320(2)	12.71810(10)	11.23374(5)	28.4430(7)	27.2058(8)	32.869(2)
α /°	90	101.2730(10)	90	90	90	90
β /°	90	94.7670(10)	94.2834(4)	90	90.472(3)	92.384(5)
γ /°	90	93.6800(10)	90	90	90	90
<i>V</i> /Å ³	5038.8(2)	1288.38(2)	2461.33(2)	10020.0(4)	9579.1(5)	4448.9(4)
<i>Z</i>	8	2	4	8	8	4
<i>D</i> _{calc} /g cm ^{−3}	1.201	1.174	1.148	1.252	1.196	1.198
<i>F</i> (000)	1968	492	920	4032	3680	1712
μ /mm ^{−1}	0.948	0.109	0.906	0.546	1.121	0.599
θ range	2.162–64.995	2.337–24.998	3.896–75.379	2.071–25.000	2.3040–68.480	1.240–26.215
Crystal size/mm	0.300 × 0.200 × 0.200	0.340 × 0.300 × 0.200	0.150 × 0.120 × 0.110	0.080 × 0.050 × 0.030	0.320 × 0.040 × 0.040	0.400 × 0.320 × 0.240
Reflns collected	66,305	9350	85,197	50,096	8821	20,791
Reflns unique	4278	9350	4659	8814	8821	8877
<i>R</i> _{int}	0.1663	0.0234	0.0468	0.0650	0.1309	0.0551
<i>R</i> ₁ / <i>wR</i> ₂ [<i>I</i> > 2 σ (<i>I</i>)]	0.0691; 0.1785	0.0420; 0.1202	0.0327; 0.0319	0.0434; 0.0925	0.0441; 0.1179	0.0386; 0.0644
<i>R</i> ₁ / <i>wR</i> ₂ (all data)	0.0828; 0.1879	0.0445; 0.1226	0.0856; 0.0850	0.0620; 0.1003	0.0510; 0.1212	0.0868; 0.0709
Parameters	300	301	281	606	551	490
GOF (<i>F</i> ²)	1.050	1.030	1.036	1.061	1.058	0.765
Largest diff. peak and hole/e.Å ^{−3}	0.348 and −0.367	0.579 and −0.339	0.268 and −0.267	0.298 and −0.412	1.063 and −0.566	0.396 and −0.358

References

- Makio, H.; Terao, H.; Iwashita, A.; Fujita, T. FI catalysts for olefin polymerization—a comprehensive treatment. *Chem. Rev.* **2011**, *111*, 2363–2449. [CrossRef]
- Redshaw, C.; Tang, Y. Tridentate ligands and beyond in group IV metal α -olefin homo-/co-polymerization catalysis. *Chem. Soc. Rev.* **2012**, *41*, 4484–4510. [CrossRef]
- Gao, J.; Zhu, D.; Zhang, W.; Solan, G.A.; Ma, Y.; Sun, W.-H. Recent progress in the application of group 1, 2 & 13 metal complexes as catalysts for the ring opening polymerization of cyclic esters. *Inorg. Chem. Front.* **2019**, *6*, 2619–2652.

4. Wei, Y.; Wang, S.; Zhou, S. Aluminum alkyl complexes: Synthesis, structure, and application in ROP of cyclic esters. *Dalton Trans.* **2016**, *45*, 4471–4485. [[CrossRef](#)] [[PubMed](#)]
5. Wu, J.; Yu, T.-L.; Chen, C.-T.; Lin, C.-C. Recent developments in main group metal complexes catalyzed/initiated polymerization of lactides and related cyclic esters. *Coord. Chem. Rev.* **2006**, *250*, 602–626. [[CrossRef](#)]
6. Fuoco, T.; Pappalardo, D. Aluminum Alkyl Complexes Bearing Salicylaldiminato Ligands: Versatile Initiators in the Ring-Opening Polymerization of Cyclic Esters. *Catalysts* **2017**, *7*, 64. [[CrossRef](#)]
7. Santoro, O.; Zhang, X.; Redshaw, C. Synthesis of biodegradable polymers: A review on the use of Schiff-base metal complexes as catalysts for the Ring Opening Polymerization (ROP) of cyclic esters. *Catalysts* **2020**, *10*, 800. [[CrossRef](#)]
8. Guo, L.-h.; Gao, H.-y.; Zhang, L.; Zhu, F.-m.; Wu, Q. An Unsymmetrical Iron(II) Bis(imino)pyridyl Catalyst for Ethylene Polymerization: Effect of a Bulky Ortho Substituent on the Thermostability and Molecular Weight of Polyethylene. *Organometallics* **2010**, *29*, 2118–2125. [[CrossRef](#)]
9. Ghaffari, A.; Behzad, M.; Pooyan, M.; Rudbari, H.A.; Bruno, G. Crystal structures and catalytic performance of three new methoxy substituted salen type nickel (II) Schiff base complexes derived from meso-1, 2-diphenyl-1, 2-ethylenediamine. *J. Mol. Struct.* **2014**, *1063*, 1–7. [[CrossRef](#)]
10. Arbaoui, A.; Redshaw, C.; Hughes, D.L. Multinuclear alkylaluminium macrocyclic Schiff base complexes: Influence of procatalyst structure on the ring opening polymerisation of epsilon-caprolactone. *Chem. Commun.* **2008**, *39*, 4717–4719. [[CrossRef](#)]
11. Hsu, C.-Y.; Tseng, H.-C.; Vandavasi, J.K.; Lu, W.-Y.; Wang, L.-F.; Chiang, M.Y.; Lai, Y.-C.; Chen, H.-Y.; Chen, H.-Y. Investigation of the dinuclear effect of aluminum complexes in the ring-opening polymerization of epsilon-caprolactone. *RSC Adv.* **2017**, *7*, 18851–18860. [[CrossRef](#)]
12. Liu, J.; Iwasa, N.; Nomura, K. Synthesis of Al complexes containing phenoxy-imine ligands and their use as the catalyst precursors for efficient living ring-opening polymerisation of epsilon-caprolactone. *Dalton Trans.* **2008**, 3978–3988. [[CrossRef](#)]
13. Zhang, W.; Wang, Y.; Sun, W.-H.; Wang, L.; Redshaw, C. Dimethylaluminium aldiminophenolates: Synthesis, characterization and ring-opening polymerization behavior towards lactides. *Dalton Trans.* **2012**, *41*, 11587–11596. [[CrossRef](#)]
14. Aeilts, S.L.; Coles, M.P.; Swenson, D.C.; Jordan, R.F.; Young, V.G. Aluminum Alkyl Complexes Containing Guanidinate Ligands. *Organometallics* **1998**, *17*, 3265–3270. [[CrossRef](#)]
15. Sarma, B.D.; Bailar, J.C., Jr. The stereochemistry of metal chelates with polydentate ligands. Part, I. *J. Am. Chem. Soc.* **1955**, *77*, 5476–5480. [[CrossRef](#)]
16. Singh, B.K.; Prakash, A.; Rajour, H.K.; Bhojak, N.; Adhikari, D. Spectroscopic characterization and biological activity of Zn(II), Cd(II), Sn(II) and Pb(II) complexes with Schiff base derived from pyrrole-2-carboxaldehyde and 2-amino phenol. *Spectrochim. Acta Part A Mol. Biomol. Spectrosc.* **2010**, *76*, 376–383. [[CrossRef](#)]
17. Jain, A.K.; Gupta, A.; Bohra, R.; Lorenz, I.-P.; Mayer, P. Synthesis and structural elucidation of some novel aluminium(III) complexes with Schiff bases: Crystal and molecular structure of $[Al(O(C_6H_4)CHNC_6H_5)_2[HO(C_6H_4)CHNC_6H_5)_2]Br$. *Polyhedron* **2006**, *25*, 654–662. [[CrossRef](#)]
18. Niu, M.J.; Li, Z.; Chang, G.L.; Kong, X.J.; Hong, M.; Zhang, Q.F. Crystal Structure, Cytotoxicity and Interaction with DNA of Zinc (II) Complexes with o-Vanillin Schiff Base Ligands. *PLoS ONE* **2015**, *10*, e0130922. [[CrossRef](#)] [[PubMed](#)]
19. Chen, W.; Li, Y.; Cui, Y.; Zhang, X.; Zhu, H.-L.; Zeng, Q. Synthesis, molecular docking and biological evaluation of Schiff base transition metal complexes as potential urease inhibitors. *Eur. J. Med. Chem.* **2010**, *45*, 4473–4478. [[CrossRef](#)]
20. Arbaoui, A.; Redshaw, C.; Sanchez-Ballester, N.M.; Elsegood, M.R.J.; Hughes, D.L. Bimetallic copper(II) and zinc(II) complexes of acyclic Schiff base ligands derived from amino acids. *Inorg. Chim. Acta* **2011**, *365*, 96–102. [[CrossRef](#)]
21. Chakraborty, B.; Banerjee, S. Synthesis, characterization, and crystal structures of cobalt(II), copper(II), and zinc(II) complexes of a bidentate iminophenol. *J. Coord. Chem.* **2013**, *66*, 3619–3628. [[CrossRef](#)]
22. Oliveira, A.; Ferreira, L.; Dias, M.; Bitzer, R.; Nascimento, M. Ring Opening Polymerization of L-Lactide with Two Different Zinc(II) Phenoxy-Imine Complexes as Initiators. *Química Nova* **2019**, *42*, 505–512. [[CrossRef](#)]
23. Wang, Y.; Zhao, W.; Liu, D.; Li, S.; Liu, X.; Cui, D.; Chen, X. Magnesium and Zinc Complexes Supported by N,O-Bidentate Pyridyl Functionalized Alkoxy Ligands: Synthesis and Immortal ROP of epsilon-CL and l-LA. *Organometallics* **2012**, *31*, 4182–4190. [[CrossRef](#)]
24. Nassar, A.M.; Hassan, A.M.; Shoeib, M.A.; El kmash, A.N. Synthesis, Characterization and Anticorrosion Studies of New Homobimetallic Co(II), Ni(II), Cu(II), and Zn(II) Schiff Base Complexes. *J. Bio-Tribo-Corros.* **2015**, *1*, 19. [[CrossRef](#)]
25. Lee, C.-L.; Lin, Y.-F.; Jiang, M.-T.; Lu, W.-Y.; Vandavasi, J.K.; Wang, L.-F.; Lai, Y.-C.; Chiang, M.Y.; Chen, H.-Y. Improvement in Aluminum Complexes Bearing Schiff Bases in Ring-Opening Polymerization of epsilon-Caprolactone: A Five-Membered-Ring System. *Organometallics* **2017**, *36*, 1936–1945. [[CrossRef](#)]
26. Wei, Y.; Song, L.; Jiang, L.; Huang, Z.; Wang, S.; Yuan, Q.; Mu, X.; Zhu, X.; Zhou, S. Aluminum complexes with Schiff base bridged bis(indolyl) ligands: Synthesis, structure, and catalytic activity for polymerization of rac-lactide. *Dalton Trans.* **2019**, *48*, 15290–15299. [[CrossRef](#)]
27. Ajellal, N.; Carpentier, J.-F.; Guillaume, C.; Guillaume, S.M.; Helou, M.; Poirier, V.; Sarazin, Y.; Trifonov, A. Metal-catalyzed immortal ring-opening polymerization of lactones, lactides and cyclic carbonates. *Dalton Trans.* **2010**, *39*, 8363–8376. [[CrossRef](#)]
28. Qin, L.; Zhang, Y.; Chao, J.; Cheng, J.; Chen, X. Four- and five-coordinate aluminum complexes supported by N, O-bidentate beta-pyrazulenolate ligands: Synthesis, structure and application in ROP of epsilon-caprolactone and lactide. *Dalton Trans.* **2019**, *48*, 12315–12325. [[CrossRef](#)]

29. Kong, W.L.; Chai, Z.Y.; Wang, Z.X. Synthesis of N,N,O-chelate zinc and aluminum complexes and their catalysis in the ring-opening polymerization of epsilon-caprolactone and rac-lactide. *Dalton Trans.* **2014**, *43*, 14470–14480. [\[CrossRef\]](#)
30. Munzeiwa, W.A.; Nyamori, V.O.; Omondi, B. N,O-Amino-phenolate Mg(II) and Zn(II) Schiff base complexes: Synthesis and application in ring-opening polymerization of epsilon-caprolactone and lactides. *Inorg. Chim. Acta* **2019**, *487*, 264–274. [\[CrossRef\]](#)
31. Mata-Mata, J.L.; Gutiérrez, J.A.; Paz-Sandoval, M.A.; Madrigal, A.R.; Martínez-Richa, A. Ring-opening polymerization of epsilon-caprolactone initiated with different ruthenium derivatives: Kinetics and mechanism studies. *J. Polym. Sci. Part A Polym. Chem.* **2006**, *44*, 6926–6942. [\[CrossRef\]](#)
32. Hammett, L.P. The Effect of Structure upon the Reactions of Organic Compounds. Benzene Derivatives. *J. Am. Chem. Soc.* **1937**, *59*, 96–103. [\[CrossRef\]](#)
33. Zhao, W.; Wang, Q.; Cui, Y.; He, J.; Zhang, Y. Living/controlled ring-opening (co)polymerization of lactones by Al-based catalysts with different sidearms. *Dalton Trans.* **2019**, *48*, 7167–7178. [\[CrossRef\]](#) [\[PubMed\]](#)
34. Rae, A.; Gaston, A.J.; Greindl, Z.; Garden, J.A. Electron rich (salen)AlCl catalysts for lactide polymerisation: Investigation of the influence of regioisomers on the rate and initiation efficiency. *Eur. Polym. J.* **2020**, *138*, 109917. [\[CrossRef\]](#)
35. Hung, W.-C.; Huang, Y.; Lin, C.-C. Efficient initiators for the ring-opening polymerization of L-lactide: Synthesis and characterization of NNO-tridentate Schiff-base zinc complexes. *J. Polym. Sci. Part A Polym. Chem.* **2008**, *46*, 6466–6476. [\[CrossRef\]](#)
36. Wang, J.; Wang, L.; Zhou, Z.; Lai, H.; Xu, P.; Liao, L.; Wei, J. Biodegradable polymer membranes applied in guided bone/tissue regeneration: A review. *Polymers* **2016**, *8*, 115. [\[CrossRef\]](#)
37. Van den Vreken, N.M.; Dubruel, P.; Verbeeck, R.M. The effect of a photopolymerizable poly (epsilon-caprolactone-co-glycolide) matrix on the cement reactions of tetracalcium phosphate and tetracalcium phosphate–monocalcium phosphate monohydrate mixtures. *J. Mater. Chem. B* **2013**, *1*, 1584–1594. [\[CrossRef\]](#)
38. Cooper, K.; Nathan, A.; Vyakarnam, M. Poly (epsilon-Caprolactone-co-Glycolide): Biomedical Applications of a Unique Elastomer. *Biodegrad. Polym. Clin. Use Clin. Dev.* **2011**, 401–415.
39. Kasperczyk, J. Copolymerization of glycolide and epsilon-caprolactone, 1. Analysis of the copolymer microstructure by means of ¹H and ¹³C NMR spectroscopy. *Macromol. Chem. Phys.* **1999**, *200*, 903–910. [\[CrossRef\]](#)
40. Meduri, A.; Fuoco, T.; Lamberti, M.; Pellicchia, C.; Pappalardo, D. Versatile Copolymerization of Glycolide and rac-Lactide by Dimethyl(salicylaldiminato)aluminum Compounds. *Macromolecules* **2014**, *47*, 534–543. [\[CrossRef\]](#)
41. Li, S. Structure-Property Relationships of Copolymers Obtained by Ring-Opening Polymerization of Glycolide and E-Caprolactone. Part 1. Synthesis and Characterization. *Biomacromolecules* **2005**, *6*, 483–488. [\[CrossRef\]](#)
42. Zheng, Y.; Turner, W.; Zong, M.; Irvine, D.J.; Howdle, S.M.; Thurecht, K.J. Biodegradable Core–Shell Materials via RAFT and ROP: Characterization and Comparison of Hyperbranched and Microgel Particles. *Macromolecules* **2011**, *44*, 1347–1354. [\[CrossRef\]](#)
43. Yang, W.; Zhao, K.Q.; Wang, B.Q.; Redshaw, C.; Elsegood, M.R.; Zhao, J.L.; Yamato, T. Manganese coordination chemistry of bis(imino)phenoxide derived [2 + 2] Schiff-base macrocyclic ligands. *Dalton Trans.* **2016**, *45*, 226–236. [\[CrossRef\]](#)
44. Wiltshire, J.T.; Qiao, G.G. Degradable core cross-linked star polymers via ring-opening polymerization. *Macromolecules* **2006**, *39*, 4282–4285. [\[CrossRef\]](#)
45. Sheldrick, G. SHELXT—Integrated space-group and crystal-structure determination. *Acta Crystallogr. Sect. A* **2015**, *71*, 3–8. [\[CrossRef\]](#) [\[PubMed\]](#)
46. Sheldrick, G. Crystal structure refinement with SHELXL. *Acta Crystallogr. Sect. C* **2015**, *71*, 3–8. [\[CrossRef\]](#)